2. Pharmacophore-based virtual screening-guided design, synthesis and biological evaluation of benzothiazole-derived thioacetamides

2.1. Design rationale and plan of work

2.1.1. Design rationale

Computational tools including high throughput virtual screening and ligand-based virtual screening i.e., LBVS techniques (e.g., pharmacophore-based design and scaffold hopping) are employed for designing a successful, safe and efficacious drug molecule. The term 'pharmacophore' is used for a set of structural features in a chemical structure that are recognized at the receptor site and are responsible for producing biological activity [115]. There are several marketed drug molecules available that act by inhibiting monoamine oxidase B (e.g., selegiline, safinamide and rasagiline) and cholinesterase inhibitors (e.g., donepezil, rivastigmine and galantamine) are used for the management of neurodegenerative diseases. Rivastigmine is a dual inhibitor of AChE and BChE while ladostigil inhibits AChE and MAO-B. Safinamide is a selective, reversible, potent inhibitor of MAO-B used in Parkinsonism and it has all the common pharmacophoric features required for MAO-B inhibition.

With an objective to identify a novel chemical template possessing potent MAO-B inhibitory properties, we have mapped safinamide as a pharmacophore model which gave rise to 6 unique pharmacophoric features (two aromatic rings, two H-bond donors, one H-bond acceptor and one hydrophobic group). This model was then utilized as a pharmacophore query using the web-based Pharmit server (http://pharmit.csb.pitt.edu/search.html/) against the ZINC15 database of 13,190,317 molecules. Further, these filtered ligands were docked using MOE software and the most active (**ZINC02181408**) ligand was used for the MD simulation study. Incidentally, the identified virtual lead MAO-B inhibitor bears a benzothiazole core moiety which is well-

known versatile pharmacophore possessing diverse pharmacological actions including multitarget inhibition properties viz., AChE and MAO-B Donia *et al*, [116]. Also, riluzole, a potential neuroprotective agent used in amyotrophic lateral sclerosis (ALS) has benzothiazole as its core heterocyclic pharmacophore [117]. This prompted us to investigate experimentally the multitarget inhibition properties of the benzothiazole-based lead compound **ZINC02181408** besides evaluating its MAO-B inhibition properties. As a part of SAR exploration, the terminal aryl ring was functionalized with variable substituents (**Figure 2.1**).

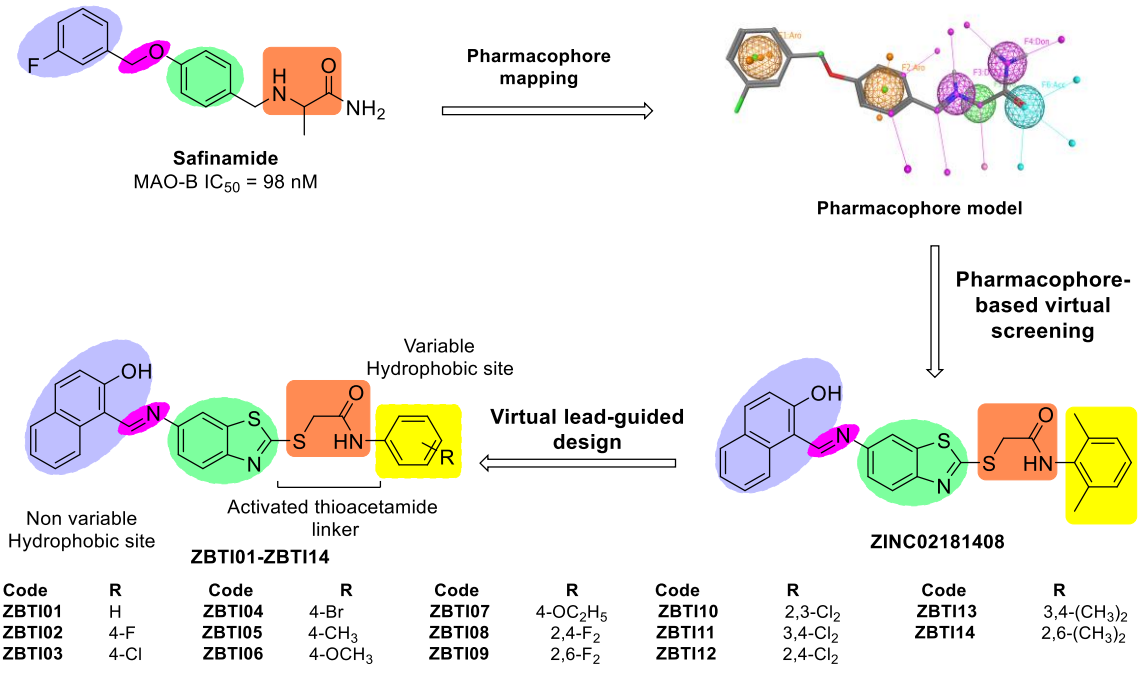

Code	R	Code	R	Code	R	Code	R	Code	R
ZBTI01	H	ZBTI04	4-Br	ZBTI07	4-OC_2H_5	ZBTI10	2,3-Cl_2	ZBTI13	3,4-$(CH_3)_2$
ZBTI02	4-F	ZBTI05	4-CH_3	ZBTI08	2,4-F_2	ZBTI11	3,4-Cl_2	ZBTI14	2,6-$(CH_3)_2$
ZBTI03	4-Cl	ZBTI06	4-OCH_3	ZBTI09	2,6-F_2	ZBTI12	2,4-Cl_2		

Figure 2.1. Design of compounds **ZBTI01-ZBTI14**

2.1.2. Objectives

- To develop a pharmacophore model using safinamide for the identification of a new MAO-B inhibitory scaffold through pharmacophore-based virtual screening.
- To design a library of virtual lead-based analogs and synthesize them using the retrosynthetic approach.

- To perform the *in vitro* biological evaluation of synthesized compounds against MAOs (MAO-A/B) and ChEs (AChE and BChE) and antioxidant, metal chelation and PAMPA-BBB penetration assay of selected compounds.
- To evaluate the lead compound(s) for their *in vitro* cellular neurotoxicity and neuroprotective potential using the SH-SY5Y cell line.
- Molecular docking, computational prediction of dual MAO/ChE ligand binding efficiency, ADMETox properties of synthesized ligands and molecular dynamic simulation studies of selected molecule.
- *In vivo* evaluation (behavioral & acute toxicity assays) of lead dual MAO/ChE inhibitors.

2.1.3. Plan of work

To accomplish the above-mentioned objectives, we employed a systematic research workflow consisting of both *in silico* and experimental methodologies which is given below (**Figure 2.2**).

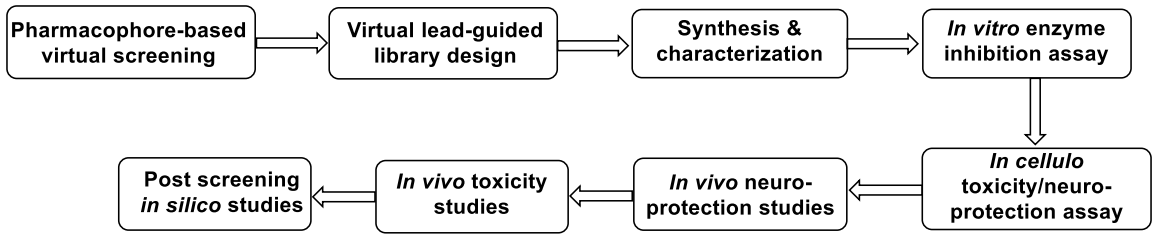

Figure 2.2. Workflow for plan of work

2.2. Experimental work

2.2.1. Tools and datasets

Various computational tools were employed for developing a pharmacophore model, query search, drug-likeness screening, PAINS filter, molecular docking and molecular dynamic simulation studies. X-ray crystal structure of monoamine oxidase-B co-crystallized with safinamide was obtained from protein data bank (https://www.rcsb.org/) [118, 119]. The pharmacophore model was generated using the pharmacophore query editor module

provided in the MOE software [120] and the model was used as a query to search the ZINC15 database through the Pharmit web server (http://pharmit.csb.pitt.edu/search.html/). The obtained hits were further screened for their drug-likeness (using DruLiTo software developed by NIPER, Mohali) and PAINS interference (https://www.cbligand.org/PAINS/login.php). Additionally, molecular docking of filtered molecules was carried out using MOE software while molecular dynamic simulation studies of the top molecule were performed by GROMACS [121]. The molecular docking studies of the virtual lead-guided designed library were performed using AutoDock Tools 4.2 while molecular dynamic simulation study of lead molecule obtained from *in vitro* enzyme inhibition studies was carried out using Desmond software [122, 123].

2.2.2. Pharmacophore-based virtual screening protocol

Several computational tools and techniques are employed to facilitate the drug discovery process. These tools include ligand-based virtual screening (LBVS) and structure-based virtual screening (SBVS). LBVS encompasses techniques like pharmacophore search, scaffold hopping, quantitative structure-activity relationship (QSAR), similarity search, chemically advanced template search and 3D geometry matching. Success stories of ligand-based drug design strategy include the discovery of $GABA_A$ agonists, dopamine receptor antagonists, angiotensin receptor antagonists (losartan and valsartan), etc. Recently, several new small molecules with selective MAO-B and AChE inhibitory potential have been identified using a ligand-based virtual screening strategy [124-129].

Protein structure of MAO-B complexed with safinamide with a resolution of 1.60 Å (PDB ID: 2V5Z) was obtained from protein data bank and utilized for the development of the pharmacophore model. Protein was cleaned by removing undesired chains, solvent and ligand molecules using the sequence editor module of MOE. Further, the protein structure was prepared using the protein preparation option provided in the sequence editor module.

Before moving to pharmacophore mapping the receptor was disabled from the system menu to clear and make ligand more visible. Additionally, the pharmacophoric features present in safinamide were mapped by selecting features and then adding them using the features option from the pharmacophore query editor module. Several pharmacophoric features, i.e., hydrogen acceptor, hydrogen donor, and aromatic center, were used to create the pharmacophore query. The generated pharmacophore query was exported in .php format. The pharmacophore query (.php) generated using MOE and receptor (MAO-B) files were loaded to the Pharmit web server (http://pharmit.csb.pitt.edu/search.html). In the hit reduction module, the maximum hit per conformer and maximum hit per molecule were set as 1 whereas the maximum total hits were left unchanged [130]. The ZINC15 library with 123,339,574 conformers of 13,190,317 molecules, selected and was screened to identify the virtual hits [131]. This screening resulted in 225 hits with RMSD $\leq$ 0.5 in the format of the structure data file (.sdf). The obtained hits were further screened for their drug-likeness and PAINS interference. The virtual hit molecules obtained from the screening of the ZINC15 database in sdf format were loaded for drug-likeness (Lipinski's filter) filter into Drug-likeness Tool (DruLiTo) developed by Department of Pharmacoinformatics NIPER, Mohali (http://www.niper.gov.in/pi_dev_tools/DruLiToWeb/DruLiTo_index.html). The physicochemical constraints such as molecular weight <500, logP <5, hydrogen bond donor <5, hydrogen bond acceptor <10, and polar surface area <100Å were applied to filter the virtual hits for further studies [132]. This filter yielded 180 hits in the sdf format. These hits were further subjected to the PAINS (Pan assay interference compounds) filter using the PAINS web server (https://www.cbligand.org/PAINS/) [118] and this filter removed 3 violator molecules and eventually yielded 177 hits in SMILES (.smi) format for further analysis. The molecules were converted into MOE's accessible format (.mdb) using MOE

2020.09. Before docking, the energy of each molecule was minimized by the 'Dock' module of the MOE using the AMBER10EHT force field.

The optimized MAO-B protein structure was loaded from the 'File' menu and was prepared using the 'Structure preparation' tool under the 'Compute' menu of the main MOE console. The structure preparation included protonation of protein in a 3D state, conformer generation, energy matrix VDW, born self-energy, isolated group energy, energy matrix ELE, and system optimization. After protein preparation the active site was zoomed in by using the 'SiteView' menu and the secondary structure of the protein was disabled from the system menu. The surface around the reference ligand was created using the 'surface' menu. The Dock module was launched from the compute menu. The MOE docking protocol was validated by running repeated docking experiments with the co-crystallized ligand, safinamide against MAO-B and the predicted ligand poses were consistent with the co-crystallized conformation of the ligand [133]. Post-validation of the docking protocol, the database of test ligands was selected and docking was performed. MOE uses Amber 10EHT as a force field for molecular docking calculations. Several placement methods (Alpha PMI, Alpha Triangle, Pharmacophore, Proxy Triangle, and Triangle Matcher) for docking but for this study we used triangle matcher as the placement method. There are two refinement methods available in MOE namely Induced Fit and Rigid Receptor; for this study, we used the induced fit refinement method. For scoring, the London dG scoring function was used as the placement scoring function while GBVI/WSA dG was used as the refinement scoring function [134-137]. After docking calculations, the binding affinity (S-score) of the top 5 stable conformers of the ligand along with refined RMSD were compiled in the form of a table in the format of a molecule database (.mdb). The more the binding affinity, the less (negative) the S-score and vice-versa. Further, a 2D interaction diagram was created by browsing the selected conformer of the ligand from the file menu of the

database viewer and the ligand interaction option provided under the compute menu. The 3D interaction diagram was created by using a 3D interaction module provided by MOE. The most active ligand was subjected to ADMET prediction using the PreADMET web-based server (https://preadmet.webservice.bmdrc.org/) along with reference molecule safinamide. The sdf file of the ligand was loaded into ChemDraw Professional 15.0 and the whole molecule was selected then the coordinates of the molecule were copied as mol text from the edit menu. The copied mol test coordinates were fed into the server's input page and submitted for calculation parameters. The predicted parameters of ADME were saved in the format of comma-separated values (.csv). The same protocol was repeated for the prediction of the toxicity parameters. The predicted parameters of ADMET include blood-brain permeability, aqueous solubility, human intestinal absorption along with the Ames test, hERG inhibition and rodent carcinogenicity.

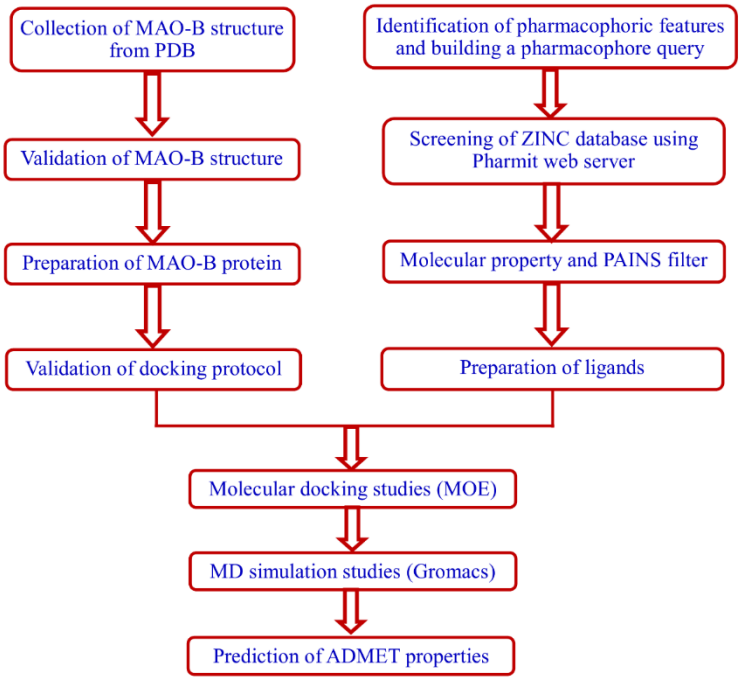

Figure 2.3. Workflow of tools and methods used for identification of virtually validated small molecule inhibitor of MAO-B.

2.2.3. Validated virtual lead-based library design

The identified virtual lead MAO-B inhibitor compound **ZINC02181408** possessed the prerequisite pharmacophoric features such as benzothiazole and phenylthioacetamide moiety. The core benzothiazole moiety is seen in reported MTDLs by Donia *et al*. (H_3R, AChE, BChE and MAO-B inhibitors), Karaca *et al.* (MAO-A/B and AChE & BChE inhibitors), [83, 116] and also in riluzole, a potential neuroprotective used in amyotrophic lateral sclerosis (ALS). Interestingly, the virtual lead inhibitor **ZINC02181408** possessed the requisite three-point pharmacophoric features (viz. two hydrophobic rings, one hydrogen bond donor, one hydrogen bond acceptor) proposed by Medvedev *et al*., [81] for MAO inhibition activity and a three-point pharmacophore model (one hydrogen bond acceptor, one hydrogen bond donor, one positively charged group, one aromatic ring) proposed by Bag *et al*., for AChE inhibition activity [138, 139]. Further, for experimental validation and SAR exploration, we have selected molecule **ZINC02181408** for designing a virtual lead-guided library of 14 compounds that were designed and synthesized by introducing different substituents at the terminal aryl ring (**Figure 2.4**). Molecule **ZINC02181408** has a 2-hydroxyl group substituted at naphthyl moiety and imine nitrogen in its proximity, which may serve as an iron-chelating pharmacophore, and can be exploited for metal chelation properties.

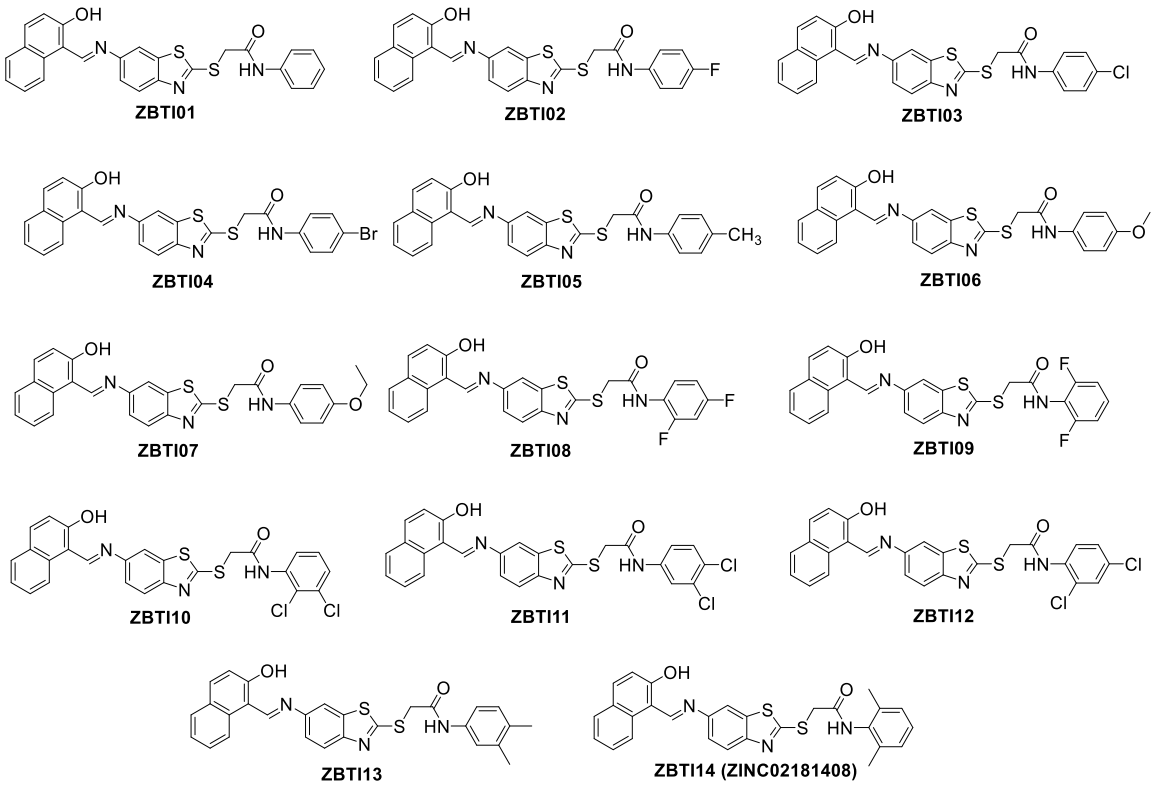

Figure 2.4. 2D chemical structures of rationally designed compounds (**ZBTI01-ZBTI14**)

2.3. Chemistry

2.3.1. Synthesis

All chemicals utilized for the synthesis of intermediates and target compounds were obtained from authentic sources and authorized chemical manufacturers and vendors. The chemicals were procured from Sigma Aldrich Chemical Private Ltd., India, Thermofisher Scientific Ltd. India, Merck India, and Sisco Research Laboratories Pvt Ltd., India, and used without further purification.

6-Amino-2-mercaptobenzothiazole and 2-hydroxy-1-naphthaldehyde coupled imine derivatives (**ZBTI01-ZBTI14**) were synthesized by the scheme discussed below (**Scheme 2.1**).

For ease of synthesis, we utilized a retrosynthetic (bond disconnection) strategy to identify synthetically accessible or easily available synthons/fragments namely, 2-hydroxy-1-naphthaldehyde, 6-amino-2-mercaptobenzothiazole and substituted aniline (**Scheme 2.1**, upper panel). Accordingly, we designed a multistep synthetic scheme (**Scheme 2.1**, lower

panel) starting from substituted aniline to accomplish the synthesis of final compounds (**ZBTI01-ZBTI14**). The detailed synthetic procedures are described in the following section.

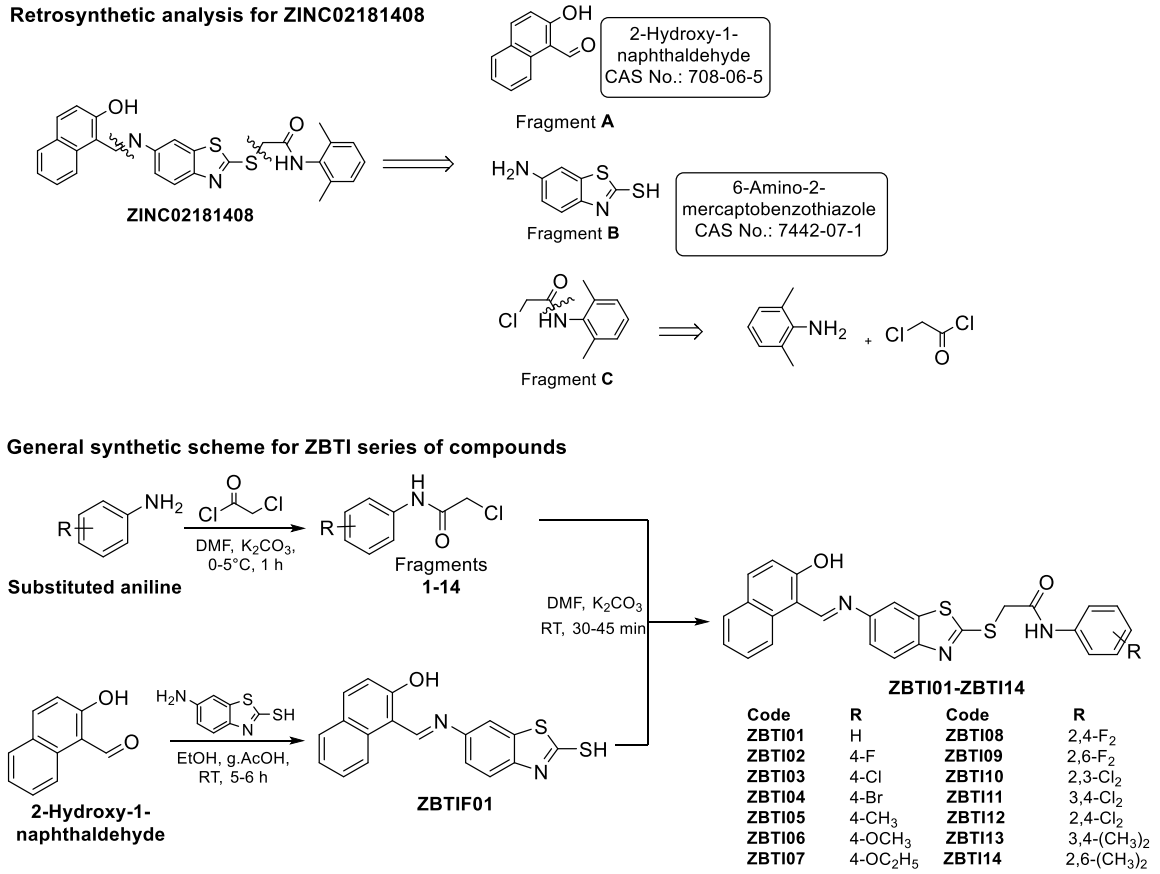

Scheme 2.1. Retrosynthetic analysis of virtual lead compound **ZINC02181408** and synthetic scheme for intermediates and final compounds **ZBTI01-ZBTI14.**

Step 1: Synthesis of phenyl chloroacetamide (1-14) fragments from substituted anilines

The powdered and activated potassium carbonate (10.0 mmol) and chloroacetyl chloride (10.0 mmol) were added to a magnetically stirred solution of substituted aniline (5.0 mmol) in dimethyl formamide (DMF, 10 mL) at 0 ˚C. The resultant reaction mixture was further stirred for about 1 h and the progress of the reaction was monitored by TLC. On completion of the reaction (as confirmed by TLC), the reaction mixture was poured on ice and an equal volume of water (50 mL) was added to quench excess chloroacetyl chloride and DMF

present in the reaction mixture. The content was stirred for about 10 min and then filtered under reduced pressure to yield a solid product [140].

Step 2: Synthesis of (*E*)-1-(((2-mercaptobenzo[*d*]thiazol-6-yl)imino)methyl)naphthalen-2-ol (ZBTIF01)

To a magnetically stirred solution of 6-amino-2-mercaptobenzothiazole (11.0 mmol) in 50 mL absolute ethanol, 2-hydroxy-1-naphthaldehyde (12.0 mmol) was added. The pH of the reaction mixture was adjusted between 5-6 by using glacial acetic acid and further stirred at room temperature for about 5-6 h. After completion of the reaction (as confirmed by TLC) it was cooled to 0 ºC and filtered under reduced pressure to obtain a brick red-colored solid product with a yield of 90 % [141].

Step 3: Synthesis of final compounds ZBTI01-ZBTI14

To a magnetically stirred solution of **ZBTIF01** (0.6 mmol) in 10 mL of DMF, powdered potassium carbonate (0.6 mmol) and acetamide fragment of substituted aniline (Fragments **1-14**, 0.6 mmol) were added and the reaction mixture was further stirred at room temperature for about 30-45 min and progress of the reaction was monitored. On completion of the reaction, the mixture was quenched with crushed ice and stirred for 10 min. The precipitated solid product was isolated by filtration under reduced pressure. All the final compounds were obtained in good yields of 67-95 % [142].

2.3.2. Physicochemical characterization

The physicochemical characterizations of synthesized compounds (**ZBTI01-ZBTI14**) were performed for retardation factor (R_f), melting point/range, solubility, and experimental LogP.

A. TLC and R_f calculation

TLC was carried out to determine the retardation factor (R_f) value of each compound. A mobile phase of 30 % ethyl acetate and 70 % *n*-hexane was used to monitor the progress of

the reaction as well as for R_f determination of final compounds. R_f is defined as the distance traveled by solute divided by the distance traveled by solvent.

R_f = Distance traveled by solute/Distance traveled by solvent

B. Determination of melting point and solubility

The melting point/range of synthesized compounds was recorded using digital melting point apparatus model IIC327 through one-end open capillary tubes and was uncorrected. Further, all the compounds were subjected to solubility analysis using a number of non-polar and polar organic solvents at ambient temperature.

C. LogP determination

The λ_{max} of compounds **ZBTI01-ZBTI14** was determined in spectroscopy grade methanol at a concentration of 10 µg/mL. The standard calibration curve for each compound was prepared by recording the absorbance of 6 different concentrations i.e., 1, 2, 4, 6, 8, 10, and 12 µg/mL in methanol at their λ_{max}. This calibration curve was further used to calculate the unknown concentration of compounds obtained after partitioning in *n*-octanol and water (maintained at pH 7.4 by phosphate buffer). The *n*-octanol was saturated with water of pH 7.4 and water was also saturated with *n*-octanol for 24 hours after vigorous shaking in the separating funnel. A weighed amount (1 mg) of the compound was added to a volumetric flask of 10 mL containing 5 mL of pre-saturated *n*-octanol and 5 mL of pre-saturated water at pH 7.4. The flasks were shaken vigorously for 25-30 min and then kept aside for 24 hours. Both layers were collected separately and the absorbance of each was taken at λ_{max} and required dilution was performed where necessary. The concentration of the compound in each layer was calculated using the calibration curve. The partition coefficient was calculated using the following formula; partition coefficient = concentration of compound in *n*-octanol layer/concentration of compound in water layer. Finally, the logarithm of the

partition coefficient was taken to arrive at the final logP value of each compound [143, 144].

2.3.3. Spectral characterization

The chemical structure of each synthesized compound was evaluated by using several spectroscopic techniques like UV-Vis spectroscopy, vibrational spectroscopy (FTIR), nuclear magnetic resonance (NMR, rotational spectroscopy) and high-resolution mass spectrometry (HRMS). The wavelength of maximum absorbance (λ_{max}) of final compounds was recorded on Agilent Cary 60 Spectrophotometer. The absorption spectra of infrared radiation were determined using the Shimadzu FTIR-8400S instrument through the KBr pressed pellet method.

^{1}H and ^{13}C NMR spectroscopic characterization was performed for all the synthesized compounds using Bruker 500 MHz FT-NMR spectrophotometer using deuterated dimethyl sulfoxide (DMSO-d_6) as a solvent. The analysis was carried out at the Central Instrument Facility (CIF), IIT (BHU), Varanasi and SATHI facility in the Central Discovery Center (CDC) Banaras Hindu University (BHU). The chemical shift values are presented in ppm (parts per million) downfield from tetramethylsilane (TMS, internal standard) and the observed coupling constant (*J*) is presented in Hertz (Hz). In ^{1}H NMR the peaks of spectra are reported as *s*- singlet, *d*- doublet, *dd*- doublet of doublet, *dt* – doublet of triplet, *ddd* – doublet of doublet of doublet, *t*- triplet and *m*- multiplet. High-resolution mass spectrometry (HRMS) characterization was performed using the X500R QTOF system in +IDA TOF mode available in the Analytical Laboratory of the Department of Chemistry, Institute of Science, Banaras Hindu University (ISc-BHU), Varanasi. The purity profile of selected compounds was evaluated using Agilent 1260 Infinity II HPLC system-equipped diode array detector available in departmental sophisticated instrument facility.

2.4. Biological studies

2.4.1. *In vitro* studies

To evaluate the dual MAO and ChE inhibitory potential of synthesized compounds, *in vitro* enzyme inhibition studies against MAOs (MAO-A & MAO-B) and ChEs (AChE & BChE) were performed. Additionally, the selected compounds were evaluated for *in vitro* antioxidant and metal chelation properties to identify their multifunctional profile. Furthermore, an *in vitro* blood-brain-barrier permeation assay was carried out to evaluate the brain-penetration capabilities along with cell-based toxicity and neuroprotection of the multifunctional molecules.

2.4.1.1. *In vitro* MAO-A/B enzyme inhibition assay

Horseradish peroxidase (HRP)-based colorimetric assay kit was purchased from Sigma-Aldrich Chemicals Private Limited (cat. no. P8125), vanillic acid was obtained from Sisco Research Laboratories Pvt. Ltd. (cat. no. 83080) while 4-aminoantipyrine was procured from Spectrochem Pvt. Ltd. Clorgyline hydrochloride (cat. no. 15925) and serotonin hydrochloride (cat. no. 33680) were procured from Cayman Chemical Company. All the chemical components were purchased through authorized local dealers.

A peroxidase-linked colorimetric assay was utilized for the determination of MAO-A/B inhibition of synthesized compounds. The assay is based on the detection of 'quinoneimine dye' formed by the reaction of vanillic acid and the oxidized product of 4-aminoantipyrine, the chromogenic substrate for this assay. The oxidation of 4-aminoantipyrine, in turn, is brought about by the action of MAO-A/B on its amine substrate i.e., serotonin (converted into 5-hydroxy indole-3-acetaldehyde, 5-HIAL) and benzylamine (converted into benzaldehyde), respectively, via the formation of the ROS (H_2O_2) through the cascade reactions (**Figure 2.5**). Rat liver mitochondrial homogenate was used as the source of MAOs (MAO-A and MAO-B). The extraction of protein was performed as per the method

described by Halt *et al.,* and protein quantification was done through Bradford protein estimation assay using bovine serum albumin as a quantification standard [145, 146]. 10 µL of test and reference compounds (20, 10, 1, 0.1 and 0.01 µM) was incubated with 40 µL of mitochondrial suspension for 20 min and then 40 µL of the chromogenic solution, 120 µL of amine substrate (serotonin 2.5 mM, benzylamine 5 mM) was added to the mixture and finally 40 µL of the assay buffer (phosphate buffer 0.2 M, pH 7.6) was added to the well and incubated at 37 ˚C for 90 min. After incubation, the absorbance of the mixture was recorded at λ 490 nm on a multimode microplate reader (BioTek Cytation 5 Imaging Reader, Agilent Technologies). Each assay was carried out in triplicate and the experiment was repeated twice. Tranylcypromine was used as a non-selective reference inhibitor whereas clorgyline and selegiline were used as a reference inhibitor of MAO-A and MAO-B, respectively.

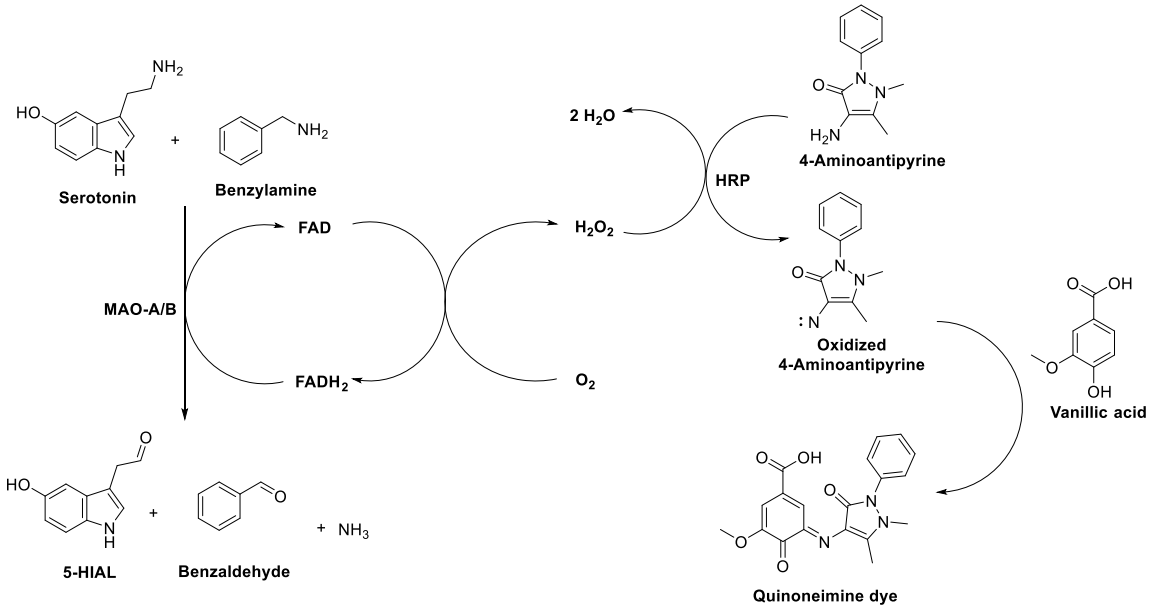

Figure 2.5. Principle of peroxidase-linked colorimetric assay

2.4.1.2. *In vitro* ChEs inhibition assay

The acetylcholinesterase sourced from *Electrophorus electricus* (electric eel) was procured from Sigma-Aldrich Chemicals Private Limited (cat. no. C2888) and S-acetylthiocholine iodide (ATCI) was obtained from Sisco Research Laboratories Pvt. Ltd. (cat. no. 38998).

Further, 5,5-dithiobis(2-nitrobenzoic acid) was purchased from Sisco Research Laboratories Pvt. Ltd. (cat. no. 32363). Ellman's method with slight modification was used for the determination of the AChE inhibitory potential of the compounds. The assay is based on measuring the change in absorbance at λ 415 nm. AChE hydrolyses the acetylthiocholine to produce thiocholine and acetate. The thiocholine reduces the dithiobis-nitrobenzoic acid (DTNB) liberating nitrothiobenzoate (**Figure 2.6**), which absorbs at λ 415 nm. Donepezil hydrochloride (cat. no. D6821) was used as a reference AChE inhibitor. The experiments were performed using 50 mM Tris-HCl buffer at pH 8.0. Initially, 10 µL of test or reference compound (20, 10, 1, 0.1, 0.01 µM) was incubated with 50 µL AChE (0.022 U/mL) for 30 min at room temperature. Further, 30 µL of the substrate (acetylthiocholine iodide, ATCI, 1.5 mM) was added and the resultant solution was again incubated for 30 min at room temperature. Lastly, 160 µL of DTNB (0.15 mM) was and the absorbance was recorded at λ 415 nm wavelength using a multimode microplate reader (BioTek Cytation 5 Imaging Reader, Agilent Technologies). Each assay was carried out in triplicate and the experiment was repeated three times. The blank well contained all the components except the enzyme and inhibitor while the control well contained all components except the inhibitor. BChE inhibition assay was performed by using *equine* serum (cat. no. C1057) as the enzyme source and butyryl thiocholine iodide (cat. no. 82366) was used as substrate (BTCI, 1.5 mM) and the same assay protocol was repeated as AChE [144].

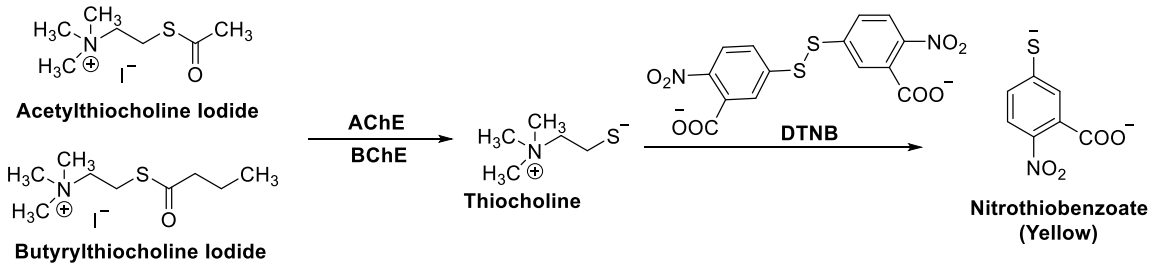

Figure 2.6 Principle involved in the AChE/BChE inhibition assay

2.4.1.3. Enzyme kinetics and reversibility assay

To investigate the inhibitory mechanism of lead MAO-B inhibitor, a double reciprocal plot was constructed between 1/[V] and 1/[S] using five different concentrations of substrate benzylamine (2.5, 5.0, 7.5, 10.0 and 15.0 mM). 10 µL of test compound at different concentrations (1, 5 and 10 µM) was pre-incubated with 40 µL of MAO protein (0.5 mg/mL) for 20 min then 40 µL chromogenic solution and 120 µL of the substrate were added followed by 40 µL of assay buffer and further incubated for 90 min. The absorbance was measured at λ 490 nm. The time-dependent reversibility study was performed to understand the type of ligand binding. For this, the test compound was pre-incubated with enzyme for different periods of time (0, 15, 30, and 60 min) and then the chromogenic solution was added to the mixture along with respective substrate (5.0 mM of benzylamine) and again incubated for 90 min and absorbance was measured at 490 nm. The obtained results were plotted as a histogram and binding type was determined [133].

To study the AChE inhibitory mechanism of the lead compound, reciprocal plots of 1/[V] versus 1/[S] were constructed using five different concentrations of the substrate acetylthiocholine iodide (ATCI) (0.5, 1.0, 1.5, 2.0, and 2.5 mM) for *ee*AChE by using Ellman's method. The lead compound (10 µL) was pre-incubated at different concentrations (1, 5, and 10 µM) with *ee*AChE (50 µL of 0.022 U/mL), and DTNB (160 µL of 0.15 mM for AChE; at 37 ºC for 30 min, followed by the addition of 30 µL of the substrate at different concentrations. The kinetic characterization of the hydrolysis of ATCI catalyzed by AChE was done spectrophotometrically using a 96-well microplate reader at λ 415 nm. The time-dependent reversibility study was carried out to understand the binding type of ligands within the enzyme active site. Compound concentration equal to two-fold of IC_{50} was preincubated with 50 µL of working enzyme concentration (0.022 U/mL) and 160 µL of DTNB for different time periods (0, 15, 30, and 60 min) and finally 30 µL of

ATCI was added and further re-incubated for 15 min after that the absorbance was recorded at λ 415 nm. The obtained results were plotted as a histogram to determine the inhibition type (reversible or irreversible) [147].

2.4.1.4. *In vitro* antioxidant assay

Oxidative stress is one of the major causes of neurodegeneration [148]. The impaired functioning of the antioxidant system of the cell leads to oxidative stress and the generation of reactive oxygen species (ROS); excessive activity of the MAO-B enzyme also causes oxidative stress and cellular damage [149]. Scavenging of these free radicals through molecules that have the ability to trap the radicals can reduce or eliminate the impact due to oxidative stress [150]. Therefore, the antioxidant potential of selected MAO/AChE inhibitor compounds was evaluated by using the DPPH (2,2-diphenyl-1-picryl-hydrazyl-hydrate) based free radical scavenging method. This method involves the conversion of DPPH to yellow-colored diphenyl picrylhydrazine in the presence of an antioxidant molecule (**Figure 2.7**). The antioxidant assay measures proton donating ability and thus determines the free radical scavenging potential of the compound. All solutions used in the DPPH assay were prepared in methanol. Five different concentrations (160, 80, 40, 20 and 10 µM) of test compounds (compounds **ZBTI02-ZBTI07** and **ZBTI10-ZBTI14**) along with donepezil, selegiline, and tranylcypromine (reference compounds) were used. In brief, 75 µL of each concentration of each test compound was loaded into a 96-well plate and additionally, 75 µL of 200 µM DPPH solution (TCI, cat. no. D4313) was transferred to each well. Finally, the microplate was incubated for 25 min at 37˚C. The absorbance of each well was recorded at wavelength 520 nm using a multimode microplate reader (BioTek Cytation 5 Imaging Reader, Agilent Technologies). Two independent experiments were performed in triplicate [147]. The percent free radical scavenging activity was calculated by equation using following formula:

$$FRS = [(Absorbance_{control} - Absorbance_{test}) / Absorbance_{control}] \times 100$$

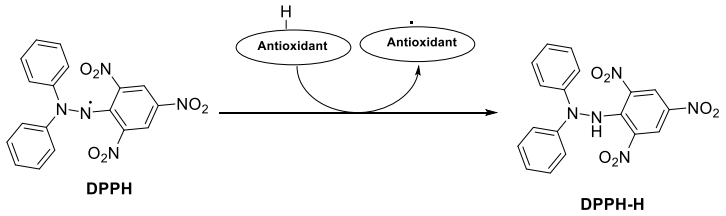

Figure 2.7. Principle of DPPH-based antioxidant assay

2.4.1.5. *In vitro* metal chelation assay

The metal chelation study of selected compounds was performed using the UV-Vis spectrophotometric method (wavelength range of λ 200-700 nm) on Cary 60 UV-Vis spectrophotometer, Agilent Technologies. A 600 µM solution of ferric (III) chloride hexahydrate ($FeCl_3.6H_2O$) was prepared in methanol and the study was performed as per the reported protocol with necessary modifications [144].

2.4.1.6. *In vitro* blood-brain-barrier permeation assay

Parallel-artificial membrane permeability assay (PAMPA) was carried out to evaluate the blood-brain-barrier accessibility of the multifunctional molecule **ZBTI13**. PAMPA assay is based on the permeability of the compound through a porcine brain lipid (PBL) coated porous membrane which mimics a blood-brain barrier. 1000 µL solution of 500 µM test compound **ZBTI13** and reference standard were prepared separately by the addition of 50 µL of 10 mM of compound dissolved in DMSO with the help of 950 µL of 1N PBS (pH 7.4). 500 µM of each test or standard compound was prepared for permeability control. Equilibrium standards (200 µM) for compound **ZBTI13** and control were prepared along with blank control (by mixing 5 µL DMSO with 245 µL of PBS). Acceptor plate (Multiscreen PVDF filter 96-well plate, Merck Millipore, Cat. MSBVN1B50) was coated with 5 µL of 20 mg/mL porcine brain lipid (CAS No.: 86088-88-2, brain lipid extract (Porcine), Avanti Polar Lipids, Inc., Cat. 141101P-100MG) dissolved in dodecane. Further, 300 µL of 500 µM compound **ZBTI13** and 500 µM of permeability controls were loaded

in duplicate to the wells of the donor plate. The acceptor plate was carefully mounted over the donor plate and left for incubation at RT or 37 ˚C for 18 h. The donor and acceptor plates were removed carefully and the content of the acceptor plate (acceptor solution) was collected for further spectroscopic analysis. 100 µL of each test or reference solution was added to the 96-well plate (Cat. # 980040) along with equilibrium control of each and blank control into the designated wells. The absorbance was recorded between λ 200 nm to 500 nm in the interval of 10 nm to arrive at the peak absorbance of the test compound **ZBTI13**. The permeability rate (P_e) was calculated using the following formula:

$$P_{e = C \times} - ln\left(1 - \frac{ODA}{ODE}\right) \text{ cm/s}$$

Where ODA is the optical density of acceptor solution minus blank, ODE is the optical density of equilibrium standard minus blank, using an 18 h incubation, C = 7.72×10^{-6}.

2.4.1.7. Cell-based neurotoxicity assay

The neurotoxicity of compound **ZBTI13** was evaluated using neuroblastoma cell line (SH-SY5Y, procured from the National Centre for Cell Science (NCCS), Pune, India) and cytotoxicity was accessed using fibroblast cells (L929, non-cancerous). The cells were cultured in DMEM culture media (Dulbecco's Modified Eagle's Medium, Himedia, cat no. AL007-500ML, HiMedia Laboratories Private Limited, India) supplemented with 10 % FBS (Fetal Bovine Serum, Himedia, cat no. RM10432) and 1 % Pen-Strep anti-biotic anti-mitotic solution. After attaining 70 % confluency the cells were counted using a hemocytometer and about 10,000 neuroblastoma cells (SH-SY5Y) and 3,000 cells of fibroblast (L929) were seeded to the well of a 96-well plate and left overnight for attachment in the incubator at 37 ˚C with 95 % humidity and 5 % CO_2. Further, neuroblastoma cells were washed with HBSS 1X solution (HiMedia Laboratories Private Limited, India, Cat. TL1155) to remove the unattached cells while fibroblast cells were washed with PBS to remove unattached cells and cell debris if any. Different concentrations

(0.1, 1, 10, 50 and 100 µM) of compound **ZBTI13** were prepared in media and cells were treated. After 24 h the MTT assay was performed to assess the percent cell viability.

3-(4,5-dimethylthiazol-2-yl)-2,5-diphenyltetrazolium bromide (MTT) assay is a popular method used for cell viability study. MTT assay is based on the principle that reduction of MTT dye (yellow color) to formazan (purple color) due to NADPH-dependent cellular oxidoreductases (**Figure 2.8**). Healthy and growing cells have the ability to reduce MTT solution to purple formazan while dead cells fail to do so [151]. A more intense purple color means more healthy cells and *vice versa*. To perform the MTT test the cells were treated with 10 % of MTT solution (5 mg/mL).

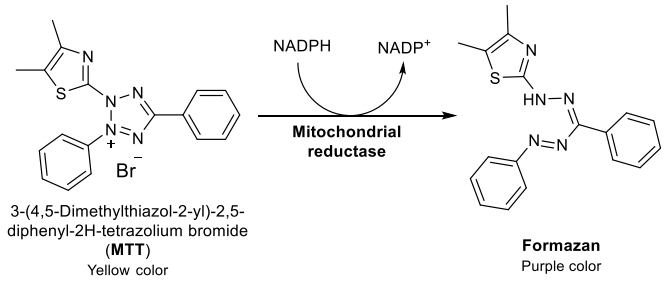

Figure 2.8. Principle and reaction of MTT assay

2.4.1.8. Neuroprotection assay using neuroblastoma cell line

The multifunctional compound **ZBTI13** was evaluated against dexamethasone-induced oxidative stress in neuroblastoma cell line (SH-SY5Y). The cells were cultured in DMEM culture media (HiMedia Laboratories Private Limited, India, Cat. AL007) and after attaining 70 % confluency it was counted using a hemocytometer and about 10,000 cells were loaded to the well of 96-well plate and left overnight for attachment. Further, cells were washed with HBSS 1X solution (HiMedia Laboratories Private Limited, India, Cat. TL1155) to remove the unattached cells. Different concentrations (0.25, 100 and 200 nM) of compound **ZBTI13** were prepared in media containing 2 µM of dexamethasone (HiMedia Laboratories Private Limited, India, Cat. TCL211) solution and cells were treated for 3 days (72 h). During the treatment, the cells were visualized for any morphological

change. Further, an MTT assay was performed to assess the percentage of cell viability and neuroprotection was inferred from the obtained data.

2.4.2. *In vivo* studies

Each experimentation was conducted as per the Committee for Control and Supervision of Experiments on Animals (CCSEA) Guideline vide Institutional Registration Number: 2123/GO/Re/S/21/CPCSEA. All the experimental protocols were pre-approved by the Institutional Animals Ethics Committee (IAEC) of the Indian Institute of Technology (Banaras Hindu University), Varanasi, India (IAEC Approval Number: IIT(BHU)/IAEC/2024/I/040). Adult female Albino mice (8-12 weeks old) weighing 30 ± 2 g were acquired from the Institutional Animal House, IMS-BHU, Varanasi, India and were accustomed for a week in a controlled environment (22 ± 1 ºC, 45-55% RH, 12/12 h light/ dark cycle) with food and water *ad libitum*.

The identified MTDL **ZBTI13** was subjected to *in vivo* animal behavior studies using adult albino mice to evaluate the *in vivo* efficacy and behavior of the molecule. *In vivo,* the neuroprotective effect of the compound was evaluated against a scopolamine-induced amnesia model using the Y-maze test. Further, the *ex vivo* biochemical analysis was performed to assess the level of different biochemicals in the brain.

2.4.2.1. Scopolamine induced amnesia model

Scopolamine (3 mg/kg), donepezil (5 mg/kg), and the test compound **ZBTI13** (5 mg/kg) was freshly prepared in a suspension of 0.3% sodium carboxymethyl cellulose. Animals were randomly divided into groups (n = 5 per group), including (i) Control group, (ii) Scopolamine group (3 mg/kg, i.p.), (iii) **ZBTI13** (5 mg/kg, p.o.), (iv) Donepezil (DNZ, 5 mg/kg, p.o.). The test compounds **ZBTI13** and donepezil were administered daily for up to 7 days. On the seventh day, scopolamine (3 mg/kg, i.p.) was administered to all groups,

except the control group, 30 min after the last dose of the test compounds or donepezil. The control group received only the vehicle. Fifteen minutes after the administration of scopolamine or vehicle, all animals were subjected to the Y-maze test [152].

2.4.2.2. Y-maze test

The Y-maze test is a widely used, simple, and sensitive method to assess spatial working memory and exploratory behavior in rodents. The impairment in short-term memory, stereotypic behavior and general locomotor activity is evaluated by the Y-maze test. The spontaneous alternation (SA) score was recorded using a three-arm maze, where each arm was separated by 120°. The three arms were labeled A, B, and C. During the test, each mouse was placed at the center of the maze and allowed to explore freely for a duration of 8 min. The entry into each arm was recorded using a video camera. Data from each mouse was analyzed to calculate the percentage of spontaneous alteration. An alteration was considered when the mouse entered three different arms in succession (e.g., ABC, ACB, BAC, etc.). The percentage of spontaneous alteration (% SA) was determined using the formula: % spontaneous alternation (SA) = [(number of alternations/total arm entries) 2] × 100. This calculation was used to assess short-term memory in the mice. Higher % SA values indicate improved memory performance and cognitive function in the animals [153].

2.4.2.3. *Ex vivo* biochemical analysis

The samples of the brain hippocampus and cortex region were collected carefully for *ex vivo* biochemical analysis after completion of the neuro-behavioral experiment and homogenized in 5 mL of 12.5 mM PBS (pH 7.4) using IKA® T10 basic ULTRA-TURRAX® homogenizer and centrifuged at 7000 rpm for 30 min at 4 ˚C. The supernatant was collected and used for analysis of biochemical parameters. First of all, the level of acetylcholine (ACh) was estimated using an acetylcholine ELISA kit (Krishgen Biosystems, India) while Ellman's colorimetric detection method was used to determine the level of cholinergic

marker, AChE. Briefly, 100 µL of obtained supernatant was incubated for 5 min with 15 mM of freshly prepared ATCI solution (100 µL). Further, 100 µL of 1.5 mM DTNB solution was added to the reaction mixture and absorbance was recorded at 415 nm. Hydrogen peroxide is converted into water and oxygen with the help of catalase enzyme (CAT). To evaluate the *in vivo* antioxidant potential of the multifunctional compound **ZBTI13**, the analyses of CAT and MDA (malondialdehyde) were performed using brain homogenate by the previously reported method by Sinha. The assay was performed using 50 µL of 0.1 M PBS (pH 7.4), 100 µL dichromate/acetic acid solution (5 % $K_2Cr_2O_7$/glacial acetic acid; 13 v/v), 50 µL of hydrogen peroxide (H_2O_2) and 50 µL of brain homogenate.

The level of malondialdehyde (MDA) was estimated by thiobarbituric acid reactive substance (TBARS) assay which is based on the spectrophotometric detection of red TBARS compound. In 96 well plates 50 µL of supernatant, 50 µL of PBS and 50 µL of 800 nM of hydrogen peroxide were incubated for 1 min at 37 ˚C. Further, the dichromate/acetic acid solution (150 µL) was added to it and boiled at 100 ˚C for about 10 min. Absorbance was measured at 570 nm using a microplate reader. The malondialdehyde (MDA), an oxidative stress biomarker of lipid peroxidation was measured using the thiobarbituric acid reactive substance (TBARS) assay. The assay protocol involved the mixing of 0.2 ml of 8.1 % sodium lauryl sulfate, 1.5 mL of 0.8 % aqueous thiobarbituric acid (TBA) solution, and 20 % glacial acetic acid (1.5 mL) added to the brain homogenate (0.2 mL). Deionized water was added to the mixtures, up to 4.0 ml and heated for 1 h at 95 ˚C; further cooling was done with tap water, and *n*-butanol and pyridine mixture (15:1 v/v; 5 mL) and 1 mL of distilled water were added and centrifuged. The organic layer was separated and 200 µL of the organic layer was added to a 96-well plate, and absorbance was taken at λ 532 nm using a microplate reader [152].

2.4.2.4. *In vivo* acute oral toxicity evaluation of compound ZBTI13

The *in vivo* acute oral toxicity compound **ZBTI13** was carried out on adult female Albino mice as per OECD guidelines 423 (Acute Toxicity Class Method) [154] for the determination of the median lethal dose (LD_{50}) of the compound. Three animals per group (n = 3) were randomly assigned to the vehicle control group (Group C), the 300 mg/kg body weight (BW) dosage group (Group B) and the 2000 mg/kg body weight (BW) dosage group (Group A). Since the toxicity profile of our test chemical was unknown, a starting dose of 300 mg/kg BW and 2000 mg/kg BW for the animals was chosen. In accordance with the proper dosing estimates, compound **ZBTI13** was suspended in a 0.5 % aqueous sodium carboxymethyl cellulose (NaCMC) solution and given orally by gavage in a single dose to the appropriate mouse groups that had fasted for two to three hours before the dose. A 0.5 % aqueous NaCMC solution was given to the vehicle control groups. The maximum volume of each dose was 0.2 mL. During the first 4 h after the dose and then every 24 h for the next 14 days, each animal was monitored separately for any changes in vital signs and outward indications of toxicity. On the 14^{th} day, the animals were humanely sacrificed by first anesthetizing them with 3 % v/v of isoflurane inhalation (Cat: R620 veterinary anesthesia machine, RWD life science, San Diego, USA). The highly perfused organs namely the brain, heart, kidney, and liver were collected and weighed separately for each animal and further histopathological study was performed to assess any kind of toxicity due to the test compound on the tissues of these organs. The organ coefficient of all the collected organs was calculated using the following formula: organ coefficient = [weight of the organ (g) / total body weight (g)] × 100. The results were then compared to the vehicle control group. The harvested organs were fixed in 1X PBS solution with 5-10 % formalin to perform a histopathological study of the perfused organs. Histological sections were then

taken from each organ, placed on a slide, and stained with hematoxylin and eosin (H & E) stain finally, examined under a microscope and microphotographs were taken.

2.5. Computational studies

2.5.1. Molecular docking

Molecular docking of the synthesized compounds was performed against all four target enzymes MAO-A (PDB ID: 2Z5X), MAO-B (PDB ID: 2V5Z), AChE (PDB ID: 4EY7) and BChE (PDB ID: 7AWG), using MOE (Molecular Operating Environment) software in preliminary virtual screening studies [119, 120, 155-157]. The docking protocol was validated using co-crystallized ligands. The protein was loaded into the MOE workspace and water molecules along with any duplicate chain were removed by using the 'Sequence Editor' module. The protein was prepared by the 'Protonate 3D' module of MOE which adds protons and optimizes the ionization state of the protein along with the determination of the lowest potential energy configuration. The active site was zoomed and undesired pocket atoms were disabled from the system manager. The surface was created around the ligand using the 'Surfaces and Maps' feature available under the 'Surface' option on the right-hand side panel. The 'Dock' module was used to load the ligand database and prepare protein from the MOE workspace. Triangle Matcher ligand placement methods were used for ligand placement while the Induced Fit method for refinement was used during docking studies. In this study, the London dG scoring function was used as the placement scoring function whereas GBVI/WSA dG was used as the refinement scoring function. From all the docked conformers, the top 5 conformers with the highest binding affinity (S-score) and lowest energy are displayed in the tabulated form (.mdb). The interactions of docked molecules were visualized by browsing the selected conformer from the database viewer and using the 'Ligand interactions' feature provided under the 'Compute' module of MOE. The 3D molecular interactions have been visualized using a 3D interaction tutorial. The

protein-ligand complexes having balanced binding affinity have been selected and exported in Maestro file format (.mae) [134-137].

The molecular docking studies of all the synthesized compounds were performed by AutoDock 4.2. The 2D structure of each molecule was sketched in ChemDraw® Professional 17.1.0.105. The drawn 2D structure was imported into Chem3D which converted it into a 3D structure and the energy minimization was performed by using MMFF94 force field. The resulting molecule was saved as a .pdb file and was used for further preparation of the molecule as a ligand for docking calculations. The co-crystallized structures of target proteins MAO-A (PDB ID: 2Z5X) MAO-B (PDB ID: 2V5Z), AChE (PDB ID: 4EY7) and BChE (PDB ID: 7AWG) were obtained from protein data bank (https://www.rcsb.org/). The obtained target protein structures were inspected for any missing residues and unwanted molecules, co-crystallized water and ligands were removed using Biovia Discovery Studio Visualizer (https://discover.3ds.com/discovery-studio-visualizer-download/). The protein was prepared by adding polar hydrogen atoms and was neutralized by adding Gasteiger charges. The AD4 atom type was assigned to the protein before saving it into .pdbqt format. The ligand molecule was prepared by choosing the number of torsions and saved into .pdbqt format. The grid was generated around the active site residues and the grid coordinates were saved into .gpf format. Further, the docking parameter file was generated by loading protein and ligand files, Genetic Algorithm (GA) was used as a searching parameter while docking calculation were performed using Lamarckian GA (4.2). The docked protein-ligand complex was visualized in Biovia

Discovery Studio Visualizer and images of 2D and 3D interaction were generated [123, 158].

2.5.2. Molecular dynamics simulation

The docked complex of the top-ranked inhibitor was carefully visualized and the top inhibitor from PBVS studies was further subjected to molecular dynamics simulation studies through GROMACS 2020 [121, 159-166]. The GROMOS96 54a7 force field was used to calculate the topology of the protein while the topology of ligands was calculated through an automated topology builder (ATB) server (https://atb.uq.edu.au/) which also uses the same force field to calculate topology [167]. A virtual cubic box was created around the system at a distance of 1 nm from the boundary of the system and the system was solvated with the SPC/E water model [168, 169]. The system was neutralized by adding chloride ions followed by energy minimization. Furthermore, the system was equilibrated in two phases, in the first phase with NVT and the second phase with NPT ensemble for 1000 ps each. Both the equilibration phases and production MD run were carried out at 310 K, 1 atm pressure, and the production MD run was performed for 150 ns by applying the time step of 2 fs and leapfrog integrator approach. The particle mesh Ewald (PME) method was used for long-range interactions while the cutoff value was set at 1.2 nm and Fourier spacing of 0.16 nm [170, 171]. The length of all the bonds was constrained by using LINCS algorithm [172]. Analysis of the results was done to obtain the RMSD, RMSF, and radius of gyration along with hydrogen bonding interactions, etc. [173, 174]. The VMD analysis scripts were used to visualize trajectory files of MD simulation. All the graphs were created in xmgrace.

Desmond molecular dynamics software (Schrodinger Release 2021.1) was used for post-screening MD simulation studies of compound **ZBTI13**. The protein-ligand complex was placed in a cubic box with the dimension of 1000 $Å^3$ and solvated with the TIP3P water

model. The forces between the atoms and molecules of the system were optimized by using the OPLS-force field in 2005. The counter ions were added to neutralize the system because the charged system is not suitable for simulation. The standard equilibration protocol provided in Desmond was used to pre-equilibrate and minimize the energy of the system before starting the production MD run. An MD simulation of 100 ns was performed for the docked protein-ligand complex using an NPT class ensemble by setting the temperature and pressure of the system as 300 K and 1.01325 bar, respectively. The check points as well as energy were written at different time intervals of 100 ps. The Maestro graphical user interface (Maestro, Schrodinger, LLC, New York, NY, 2021) was employed for the preparation of input files as well as for analysis and visualization of the results [15, 122].

2.5.3. Ligand binding efficiency

Ligand binding efficiency of all the compounds **ZBTI01-ZBTI14** and reference inhibitors (clorgyline, selegiline and donepezil) was calculated by feeding IC_{50} value and number of heavy atoms using MedChem calculators web server (http://www.vulpinescience.co.uk/uploads/MedChem%20Calculators_Ver3.2/MedChem%20Calculators.htm) accessed on 22 April 2024 [175].

2.5.4. Prediction of ADMET properties

All the candidate compounds were subjected to the *in silico* screening of ADMET (absorption, distribution, metabolism, excretion and toxicity) properties. A web-based server 'PreADMET' utilizes various algorithms for prediction ADME and toxicity prediction (https://preadmet.bmdrc.kr/). The molecular coordinates of each molecule were generated and copied as mol text from the edit menu in ChemDraw Professional 17.0 software (https://www.perkinelmer.com) [176, 177]. The predicted parameters of ADME were saved in the format of comma-separated values (.csv). The same protocol was repeated for the prediction of the toxicity parameters. The predicted parameters of ADMET

include blood-brain permeability, aqueous solubility, human intestinal absorption along with the Ames test, hERG inhibition and rodent carcinogenicity.

2.6. Results and discussion

2.6.1. Pharmacophore-based virtual screening (PBVS) studies

Safinamide is a selective reversible MAO-B inhibitor that consists of two aromatic rings, one carbonyl group, one secondary amine, and one primary amine group. Pharmacophore query was developed through MOE 2020.09 by mapping these groups to screen the database for potential virtual hits. The identified pharmacophoric features (**Figure 2.9**) include; two aromatic moieties (F1 and F2), two hydrogen bond donors (F3 and F4), a small hydrophobic site (F5), and a hydrogen bond acceptor (F6).

The pharmacophore query developed by MOE 2020.09 was used against the ZINC15 database via the Pharmit webserver to generate the potential virtual hits. The database search was set to one conformer per molecule and one molecule per hit and RMSD was set to 0.5 Å which resulted in 225 hits. The identified hit molecules belonged to diverse chemical scaffolds *viz.* benzothiazole (40 hits), benzimidazole (11 hits), pyrazole (4 hits), furan (14 hits), arylamine (43 hits), benzyloxy (30 hits), pyridine (9 hits), triazole (4 hits), phthalimide (2 hits), and others (20 hits) [131].

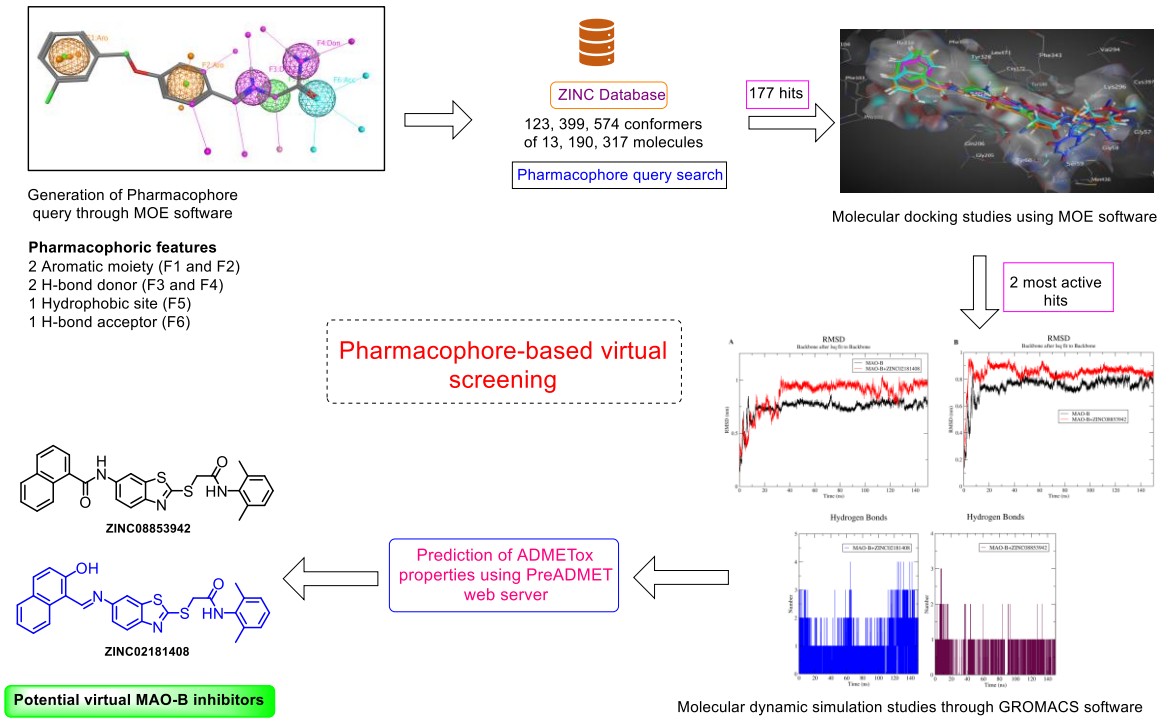

Figure 2.9. Results of pharmacophore-based virtual screening

2.6.2. Validation of virtual lead by molecular docking and MD simulation

Based on molecular docking score and binding orientation, molecule **ZINC02181408** was selected for molecular dynamic simulation studies. Molecule **ZINC02181408** displayed well-accommodated stabilization within the active site during simulation. In addition to preserving important contacts from molecular docking, the creation of new hydrogen bonding and hydrophobic interactions confirms ligand binding. (**Figure 2.10**). The molecule **ZINC02181408** exhibited moderate and low permeability for Caco2 cells and MDCK cells, respectively. The negative values of *in vitro* skin permeability indicate that the molecule is not suitable for transdermal administration. The compound **ZINC02181408** shows more than 87 % predicted human intestinal absorption (HIA) and moderate BBB permeability of 1.99. Furthermore, the predicted plasma protein binding of **ZINC02181408** was 58.80 % indicating reduced excretion rate and enhanced half-life. The plasma protein binding of the reference drug safinamide (**ZINC53084692**) was predicted to be 89.45 % and for the test ligand, it was 58.80 %. Safinamide was predicted as an

inhibitor of the enzyme CYP3A4 whereas the test ligand molecule **ZINC02181408** was predicted as a non-inhibitor against CYP2C9, CYP2C19 and CYP3A4 enzymes (**Table 2.1**).

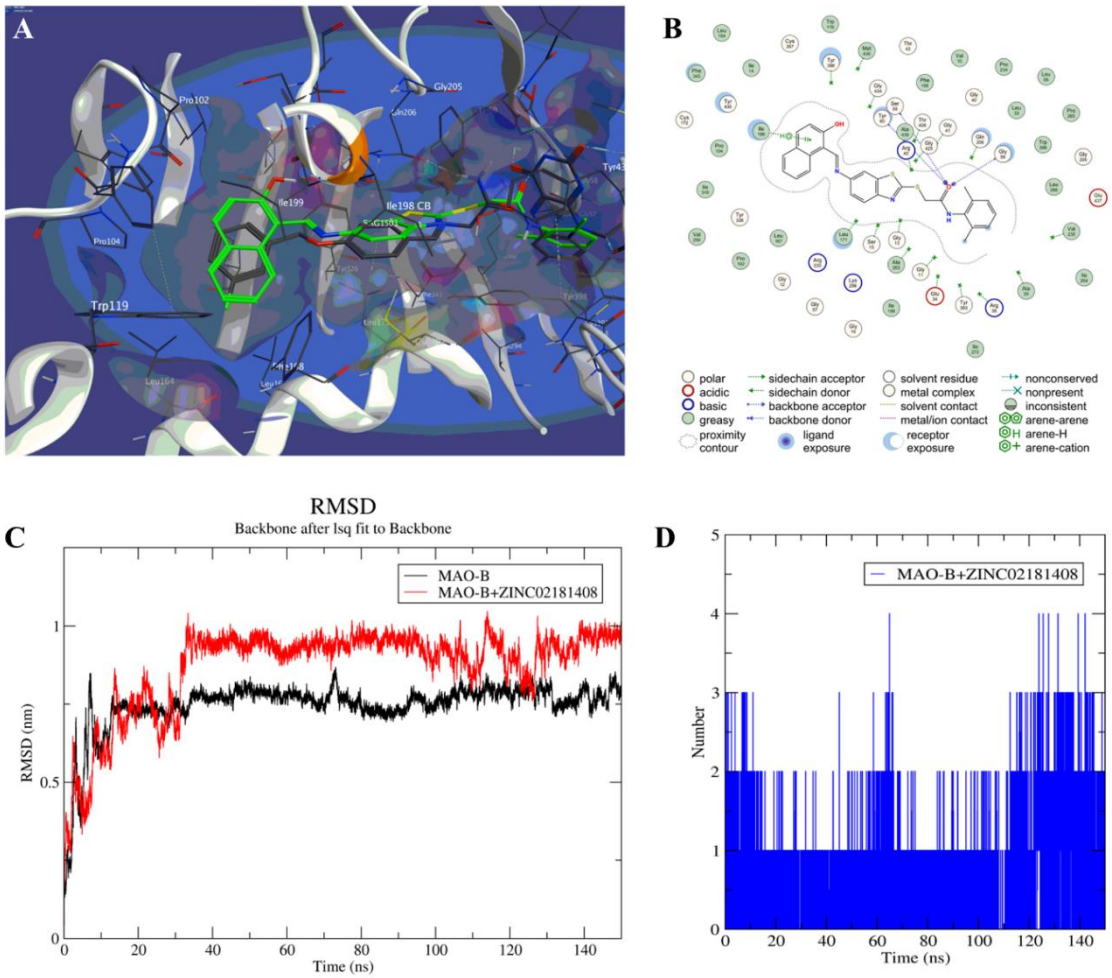

Figure 2.10. A) 3D molecular interactions of **ZINC02181408** (green) and safinamide (black) with the active site residues of MAO-B. The isoalloxazine ring of FAD is displayed as black sticks at the right; B) 2D interaction diagram of **ZINC02181408** with MAO-B active site residues; C) RMSD graph of MAO-B apoprotein (black) and **ZINC02181408**-MAO-B complex (red); D) Hydrogen bonding graph showing the number of H-bonds formed between **ZINC02181408** with active site residues of MAO-B at different period.

Table 2.1. PreADMET server predicted pharmacokinetic properties

Compound code	HIA (%)	Caco2 (nm/s)	MDCK (nm/s)	SP (log K_p, cm/h)	BBB	PPB (%)	CYP2C9 inhibition	CYP2C19 inhibition	CYP3A4 inhibition
ZBTI14 (ZINC02181408)	87.72	27.74	0.13	-3.88	1.99	58.80	Non	Non	Non

SAG (ZINC53084692)	93.59	10.27	16.90	-3.11	0.13	89.45	Non	Non	Inhibitor

HIA: Human Intestinal Absorption [0-20 (poor), 20-70 (moderate), 70-100 (well)], **Caco2**: *In-vitro* Caco2 cell permeability [<4 (low), 4-70 (moderate), >70 (high)], **MDCK**: Maden Darby Canine Kidney cell permeability [<25 (low), 25-500 (moderate), >500 (high)], **SP**: Skin permeability, **BBB**: Blood-brain-barrier permeability (C_{brain}/C_{blood}), **PPB**: *In-vitro* plasma protein binding.

2.7. Chemistry

2.7.1. Synthesis

Benzothiazole-derived thioacetamides (compounds **ZBTI01-ZBTI14**) were synthesized by using methods described in **Scheme 1.1**. Acetamides of different substituted anilines were synthesized by reacting with chloroacetyl chloride in *N*,*N*-dimethylformamide (DMF) in the presence of powdered potassium carbonate (fragments **1-14**). Imine derivative (**ZBTIF01**) of 6-amino-2-mercaptobenzothiazole was synthesized using 2-hydroxy-1-naphthaldehyde in absolute ethanol in the presence of catalytic glacial acetic acid. Further, the final compounds (**ZBTI01-ZBTI14**) were synthesized in DMF from acetamide fragments of substituted anilines (fragments **1-14**) and imine intermediate (**ZBTIF01**) in the presence of potassium carbonate with a yield of 67-95 %. The final compounds of the **ZBTI series** derived from 6-amino-2-mercaptobenzothiazole (**ZBTI01-ZBTI14**) were synthesized by the reaction of imine of 6-amino-2-mercaptobenzothiazole and 2-hydroxy-1-naphthaldehyde with suitable acetamide fragment of substituted aniline as per methods already described in the experimental section.

2.7.2. Physicochemical characterization of final compounds

All the synthesized final compounds were characterized by physicochemical and spectroscopic techniques. The obtained analytical results are in complete support of the composition of the compounds and provided in the experimental section. The synthesized compounds from imine of 6-amino-2-mercaptobenzothiazole and 2-hydroxy-1-

naphthaldehyde (**ZBTIF01)** were obtained in good yield ranging from 67 to 95 % as powdered solid. The calculated logP of compounds ranges from 5.76 to 7.98 (**Table 2.2**).

Table 2.2. Physicochemical characterization results of compounds **ZBTI01-ZBTI14**

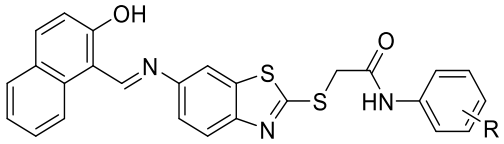

ZBTI01-ZBTI14

Compd. code	R	MW	ClogP[a]	Yield (%)	MP (°C)	R_f[b]	Solubility	Appearance
ZBTI01	H	469.57	6.33	67	185-187	0.91	DMF, DMSO	Brick red solid
ZBTI02	4-F	487.56	6.73	71	196-198	0.81	-do-	Orange solid
ZBTI03	4-Cl	504.01	7.3	77	201-203	0.75	-do-	Orange solid
ZBTI04	4-Br	548.47	7.45	95	243-245	0.54	-do-	Dark orange solid
ZBTI05	4-CH_3	483.6	6.83	92	159-161	0.88	-do-	Orange solid
ZBTI06	4-OCH_3	499.6	6.41	91	180-182	0.6	-do-	Brown solid
ZBTI07	4-OC_2H_5	513.63	6.94	89	196-198	0.62	-do-	Light orange solid
ZBTI08	2,4-F_2	505.55	6.36	74	213-215	0.8	-do-	Dark orange solid
ZBTI09	2,6-F_2	505.55	5.76	85	202-204	0.78	-do-	Orange solid
ZBTI10	2,3-Cl_2	538.46	7.13	73	209-211	0.6	-do-	Brick red solid
ZBTI11	3,4-Cl_2	538.46	7.98	78	207-209	0.66	-do-	Light orange solid
ZBTI12	2,4-Cl_2	538.46	7.25	68	201-203	0.91	-do-	Dark orange solid
ZBTI13	3,4-$(CH_3)_2$	497.63	7.28	77	149-151	0.78	-do-	Dark orange solid
ZBTI14	2,6-$(CH_3)_2$	497.63	6.03	81	206-208	0.74	-do-	Orange solid

[a] Calculated logP values from ChemDraw 17.1.0; [b] TLC mobile phase: ethyl acetate**:** *n*-hexane (4:6).

2.7.3. Spectral characterization of final compounds

Conversion of the amine group of aniline to amide resulted in a signal near δ 8.29 ppm due to NH. Further, the synthesis of imine fragment (**ZBTIF01**) was also confirmed through NMR spectroscopy which shows a signal at δ 15.60 ppm due to the hydroxyl group at naphthyl moiety and another signal near δ 10 ppm due to imine proton. The signal due to

the terminal SH group was observed near δ 14 ppm which disappeared in the NMR spectrum of final compounds indicating the formation of thioacetamides (**ZBTI01-ZBTI14**) from acetamide fragments (**1-14**) and imine fragment (**ZBTIF01**). The synthesis of acetamides from substituted anilines was confirmed by stretching vibrations at ν 3213-3268 cm^{-1} due to the NH bond in final compounds (**ZBTI01-ZBTI14**). Further, the stretching vibrations due to carbonyl appeared at ν 1620-1622 cm^{-1} while stretching due to imine (C=N) was observed at ν 1651-1700 cm^{-1}. ^{1}H and ^{13}C NMR spectroscopy shows a peak due to methylene at δ 4.22-4.49 ppm and δ 36.22-38.31 ppm, respectively. The signal due to imine C-H was confirmed at δ 8.37-9.96 ppm in proton NMR spectroscopy. The residual solvent peak was observed at δ 2.50 ppm while the peak due to moisture was observed near δ 3.35 ppm. The obtained HRMS spectra of compounds **ZBTI01-ZBTI14** showed an accuracy between 0.0000 ppm to 0.0050 ppm from the calculated $(M+H)^{+}$ mass of the compounds. The obtained physicochemical and spectral data of intermediates and final compounds are summarized below. The HPLC purity of selected compounds (**ZBTI03**, **ZBTI13** and **ZBTI14**) was obtained between 97.89 to 98.36 %.

2-chloro-*N*-(3,4-dichlorophenyl)acetamide (Fragment 11): White solid; Yield: 83%; MP: 95-97 ˚C; R_f: 0.52 in 20 % ethyl acetate-*n*-hexane; ^{1}H NMR (500 MHz, $CDCl_3$) δ 8.29 (s, 1H), 7.81 (d, J = 2.4 Hz, 1H), 7.50 – 7.36 (m, 2H), 4.21 (s, 2H); ^{13}C NMR (126 MHz, $CDCl_3$) δ 163.96, 136.09, 133.04, 130.69, 128.64, 121.80, 119.29, 42.79.

(*E*)-1-(((2-mercaptobenzo[*d*]thiazol-6-yl)imino)methyl)naphthalen-2-ol (ZBTIF01): Brick red solid; Yield: 73 %; MP: 171-173 ˚C; R_f: 0.71 in 40 % ethyl acetate-*n*-hexane; ^{1}H NMR (500 MHz, DMSO-d_6) δ 15.60 (d, J = 3.5 Hz, 1H), 13.87 (s, 1H), 9.72 (d, J = 3.4 Hz, 1H), 8.52 (d, J = 8.5 Hz, 1H), 8.07 (d, J = 2.1 Hz, 1H), 7.96 (d, J = 9.1 Hz, 1H), 7.83 (d, J = 6.4 Hz, 1H), 7.69 – 7.53 (m, 2H), 7.44 – 7.33 (m, 2H), 7.08 (d, J = 9.1 Hz, 1H); ^{13}C NMR

(126 MHz, DMSO-d_6) δ 190.11, 168.35, 157.09, 142.17, 140.32, 136.90, 133.37, 131.24, 129.50, 128.53, 127.42, 124.09, 121.72, 121.66, 120.97, 113.77, 113.45, 109.43.

(*E*)-2-((6-(((2-hydroxynaphthalen-1-yl)methylene)amino)benzo[*d*]thiazol-2-yl)thio)-*N*-phenylacetamide (ZBTI01): Brick red solid; Yield: 67 %; MP: 185-187 ˚C; R_f: 0.91 in 30 % ethyl acetate-*n*-hexane; FTIR (KBr, *v,* cm^{-1}): 3261 (N-H str), 3054 (aromatic C-H str), 1656 (C=N str), 1621 (C=O str), 1443 (aliphatic CH_2 bend), 1324 (C-O); ^{1}H NMR (500 MHz, DMSO-d_6) δ 15.71 (s, 1H), 10.46 (s, 1H), 9.77 (s, 1H), 8.54 (d, J = 8.2 Hz, 1H), 8.38 (d, J = 2.1 Hz, 1H), 7.97 (d, J = 9.3 Hz, 1H), 7.91 (d, J = 8.7 Hz, 1H), 7.83 (d, J = 7.9 Hz, 1H), 7.74 (dd, J = 8.7, 2.3 Hz, 1H), 7.65 – 7.54 (m, 3H), 7.42 – 7.30 (m, 3H), 7.12 – 7.04 (m, 2H), 4.43 (s, 2H); ^{13}C NMR (126 MHz, DMSO-d_6) δ 169.26, 166.83, 165.62, 157.02, 151.63, 141.94, 139.24, 137.13, 136.68, 133.47, 129.51, 129.34, 128.57, 127.35, 124.12, 122.12, 121.98, 120.98, 119.68, 113.81, 109.39, 38.31; HRMS Calcd for $C_{26}H_{19}N_3O_2S_2$ $(M+H)^+$ 470.0997, found 470.0991.

(*E*)-*N*-(4-fluorophenyl)-2-((6-(((2-hydroxynaphthalen-1-yl)methylene)amino)benzo[*d*]thiazol-2-yl)thio)acetamide (ZBTI02): Orange solid; Yield: 71 %; MP: 196-198 ˚C; R_f: 0.81 in 30 % ethyl acetate-*n*-hexane; FTIR (KBr, *v,* cm^{-1}): 3430 (O-H str), 3057 (aromatic C-H str), 1653 (C=N str), 1622 (C=O str), 1507 (aromatic C=C str.) 1212 (C-F str); ^{1}H NMR (500 MHz, DMSO-d_6) δ 15.70 (s, 1H), 10.53 (s, 1H), 9.77 (d, J = 4.0 Hz, 1H), 8.54 (d, J = 8.1 Hz, 1H), 8.39 (s, 1H), 7.97 (d, J = 9.3 Hz, 1H), 7.91 (d, J = 8.7 Hz, 1H), 7.83 (d, J = 6.6 Hz, 1H), 7.74 (d, J = 10.8 Hz, 1H), 7.63 (dd, J = 9.2, 5.0 Hz, 2H), 7.57 (t, J = 6.9 Hz, 1H), 7.39 (t, J = 7.5 Hz, 1H), 7.18 (t, J = 8.9 Hz, 2H), 7.08 (d, J = 9.2 Hz, 1H), 4.42 (s, 2H); ^{13}C NMR (126 MHz, DMSO-d_6) δ 169.31, 166.79, 165.58, 156.95, 151.61, 141.89, 136.89, 136.67, 135.66, 135.41, 133.47, 129.36, 128.50 128.25, 127.34, 124.11, 122.03, 121.73, 121.26, 120.99,116.03, 115.86, 113.80, 109.38, 38.19; HRMS Calcd for $C_{26}H_{18}FN_3O_2S_2$ $(M+H)^+$ 488.0902, found 488.0922.

(*E*)-*N*-(4-chlorophenyl)-2-((6-(((2-hydroxynaphthalen-1-yl)methylene)amino)benzo[*d*]thiazol-2-yl)thio)acetamide (ZBTI03): Orange solid; Yield: 77 %; MP: 201-203 ˚C; R*f*: 0.75 in 30 % ethyl acetate-*n*-hexane; FTIR (KBr, *v,* cm^{-1}): 3431 (O-H str), 3257 (N-H str), 3054 (aromatic C-H str), 1654 (C=N str), 1622 (C=O str), 1544 (aromatic C=C), 745 (C-Cl str); ^{1}H NMR (500 MHz, DMSO-d_6) δ 15.70 (s, 1H), 10.61 (s, 1H), 9.76 (d, J = 4.0 Hz, 1H), 8.54 (d, J = 8.4 Hz, 1H), 8.38 (s, 1H), 7.97 (d, J = 9.2 Hz, 1H), 7.90 (d, J = 8.5 Hz, 1H), 7.83 (d, J = 8.1 Hz, 1H), 7.74 (d, J = 8.7 Hz, 1H), 7.65 (d, J = 9.0 Hz, 2H), 7.57 (t, J = 7.7 Hz, 1H), 7.43 – 7.36 (m, 3H), 7.07 (d, J = 9.2 Hz, 1H), 4.43 (s, 2H); ^{13}C NMR (126 MHz, DMSO-d_6) δ 165.84, 157.03, 151.60, 141.96, 138.20, 137.12, 136.69, 133.47, 129.51, 129.26, 128.57, 127.69, 127.35, 124.09, 122.13, 121.97, 121.24, 120.98, 113.83, 109.39, 38.26; HRMS Calcd for $C_{26}H_{18}ClN_3O_2S_2$ $(M+H)^+$ 504.0607, found 504.0603; HPLC purity: 97.55 %.

(*E*)-*N*-(4-bromophenyl)-2-((6-(((2-hydroxynaphthalen-1-yl)methylene)amino)benzo[*d*]thiazol-2-yl)thio)acetamide (ZBTI04): Dark orange solid; Yield: 95 %; MP: 243-245 ˚C; R*f*: 0.54 in 30 % ethyl acetate-*n*-hexane; FTIR (KBr, *v,* cm^{-1}): 3245 (N-H str), 3048 (aromatic C-H str), 1651 (C=N str), 1621 (C=O str), 1536 (aromatic C=C), 500 (aromatic C-Br str); ^{1}H NMR (500 MHz, DMSO-d_6) δ 15.70 (s, 1H), 10.62 (s, 1H), 9.76 (s, 1H), 8.55 (s, 1H), 8.37 (s, 1H), 7.96 (d, J = 9.3 Hz, 1H), 7.90 (d, J = 8.7 Hz, 1H), 7.83 (d, J = 7.9 Hz, 1H), 7.73 (d, J = 8.7 Hz, 1H), 7.59 (t, J = 9.1 Hz, 3H), 7.52 (d, J = 8.9 Hz, 2H), 7.38 (t, J = 7.4 Hz, 1H), 7.07 (d, J = 9.0 Hz, 1H), 4.43 (s, 2H); ^{13}C NMR (126 MHz, DMSO-d_6) δ 169.25, 166.69, 165.87, 157.00, 151.60, 141.95, 138.61, 137.11, 136.69, 133.47, 132.17, 129.51, 128.56, 127.35, 124.08, 121.97, 121.61, 120.97, 115.72, 113.81, 109.39, 38.29; HRMS Calcd for $C_{26}H_{18}BrN_3O_2S_2$ $(M+H)^+$ 548.0102, found 548.0100.

(*E*)-2-((6-(((2-hydroxynaphthalen-1-yl)methylene)amino)benzo[*d*]thiazol-2-yl)thio)-*N*-(*p*-tolyl)acetamide (ZBTI05): Orange solid; Yield: 92 %; MP: 159-161 ˚C; R_f: 0.88 in 30 % ethyl acetate-*n*-hexane; FTIR (KBr, *v,* cm^{-1}): 3439 (O-H str), 3055 (aromatic C-H str), 1653 (C=N str), 1622 (C=O str), 1542 (aromatic C=C str); ^{1}H NMR (600 MHz, DMSO-d_6) δ 15.71 (s, 1H), 10.37 (s, 1H), 9.77 (s, 1H), 8.53 (s, 1H), 8.38 (s, 1H), 7.96 (d, J = 9.2 Hz, 1H), 7.90 (d, J = 6.8 Hz, 1H), 7.83 (d, J = 7.9 Hz, 1H), 7.73 (d, J = 8.6 Hz, 1H), 7.57 (t, J = 7.7 Hz, 1H), 7.49 (d, J = 6.6 Hz, 2H), 7.38 (t, J = 7.5 Hz, 1H), 7.14 (d, J = 7.1 Hz, 2H), 7.07 (d, J = 9.2 Hz, 1H), 4.41 (s, 2H), 2.26 (s, 3H); ^{13}C NMR (151 MHz, DMSO-d_6) δ 169.30, 166.88, 165.35, 157.00, 151.63, 141.89, 137.14, 136.74, 136.66, 133.47, 133.08, 129.70, 129.51, 128.58, 127.34, 124.10, 122.12, 122.00, 120.97, 119.67, 113.81, 109.37, 38.28, 20.93; HRMS Calcd for $C_{27}H_{21}N_3O_2S_2$ $(M+H)^+$ 484.1153, found 484.1160.

(*E*)-2-((6-(((2-hydroxynaphthalen-1-yl)methylene)amino)benzo[*d*]thiazol-2-yl)thio)-*N*-(4-methoxyphenyl)acetamide (ZBTI06): Brown solid; Yield: 91 %; MP: 180-182 ˚C; R_f: 0.60 in 30 % ethyl acetate-*n*-hexane; FTIR (KBr, *v,* cm^{-1}): 3432 (O-H str), 3055 (aromatic C-H str), 1652 (C=N str), 1621 (C=O str), 1544 (aromatic C=C str); ^{1}H NMR (500 MHz, DMSO-d_6) δ 15.71 (s, 1H), 10.33 (s, 1H), 9.77 (s, 1H), 8.55 (d, J = 8.1 Hz, 1H), 8.39 (s, 1H), 7.97 (d, J = 9.0 Hz, 1H), 7.91 (d, J = 8.7 Hz, 1H), 7.83 (d, J = 9.5 Hz, 1H), 7.74 (d, J = 10.8 Hz, 1H), 7.60 – 7.55 (m, 1H), 7.52 (d, J = 9.0 Hz, 2H), 7.38 (t, J = 7.4 Hz, 1H), 7.08 (d, J = 9.2 Hz, 1H), 6.91 (d, J = 9.2 Hz, 2H), 4.39 (s, 2H), 3.73 (s, 3H); ^{13}C NMR (126 MHz, DMSO) δ 169.34, 166.89, 165.08, 156.93, 155.94, 151.63, 141.83, 136.66, 133.47, 132.39, 129.57, 129.43, 128.61, 128.51, 127.33, 124.05, 122.04, 121.97, 121.23, 121.00, 114.51, 114.38, 113.82, 113.71, 109.36, 55.56, 38.22; HRMS Calcd for $C_{27}H_{21}N_3O_3S_2$ $(M+H)^+$ 500.1102, found 500.1103.

(*E*)-*N*-(4-ethoxyphenyl)-2-((6-(((2-hydroxynaphthalen-1-yl)methylene)amino)benzo[*d*]thiazol-2-yl)thio)acetamide (ZBTI07): Light orange solid; Yield: 89 %; MP: 196-198 ˚C; R_f: 0.62 in 30 % ethyl acetate-*n*-hexane; FTIR (KBr, *v,* cm^{-1}): 3436 (O-H str), 3262 (N-H str), 3066 (aromatic C-H str), 1658 (C=N str), 1620 (C=O str), 1544 (aromatic C=C str); ^{1}H NMR (500 MHz, DMSO-d_6) δ 15.71 (s, 1H), 10.31 (s, 1H), 9.77 (d, J = 4.0 Hz, 1H), 8.55 (d, J = 8.2 Hz, 1H), 8.39 (s, 1H), 7.97 (d, J = 9.2 Hz, 1H), 7.91 (d, J = 8.5 Hz, 1H), 7.83 (d, J = 6.4 Hz, 1H), 7.76 – 7.72 (m, 1H), 7.61 – 7.54 (m, 1H), 7.50 (d, J = 9.0 Hz, 2H), 7.39 (t, J = 7.5 Hz, 1H), 7.08 (d, J = 9.2 Hz, 1H), 6.89 (d, J = 9.0 Hz, 2H), 4.39 (s, 2H), 3.99 (q, J = 7.0 Hz, 2H), 1.31 (t, J = 7.0 Hz, 3H); ^{13}C NMR (126 MHz, DMSO) δ 169.27, 166.91, 165.05, 156.97, 155.22, 151.64, 141.84, 136.66, 133.47, 132.28, 129.16, 128.37, 127.34, 122.04, 121.25, 120.25, 115.04, 109.38, 106.98, 100.15, 63.56, 39.89, 15.17; HRMS Calcd for $C_{28}H_{23}N_3O_3S_2$ $(M+H)^+$ 514.1261, found 514.1269.

(*E*)-*N*-(2,4-difluorophenyl)-2-((6-(((2-hydroxynaphthalen-1-yl)methylene)amino)benzo[*d*]thiazol-2-yl)thio)acetamide (ZBTI08): Dark orange solid; Yield: 74 %; MP: 213-215 ˚C; R_f: 0.80 in 30 % ethyl acetate-*n*-hexane; FTIR (KBr, *v,* cm^{-1}): 3439 (O-H str), 3253 (N-H str), 3030 (aromatic C-H str), 1684 (C=N str), 1621 (C=O str), 1550 (aromatic C=C str) 1095 (aromatic C-F str); ^{1}H NMR (500 MHz, DMSO-d_6) δ 15.71 (s, 1H), 10.29 (s, 1H), 9.76 (s, 1H), 8.54 (d, J = 8.5 Hz, 1H), 8.37 (s, 1H), 7.95 (d, J = 9.2 Hz, 1H), 7.92 – 7.84 (m, 2H), 7.82 (d, J = 7.9 Hz, 1H), 7.74 (d, J = 8.7 Hz, 1H), 7.57 (t, J = 7.6 Hz, 1H), 7.42 – 7.31 (m, 2H), 7.07 (d, J = 9.0 Hz, 2H), 4.46 (s, 2H); ^{13}C NMR (126 MHz, DMSO-d_6) δ 169.28, 166.73, 166.40, 156.96, 153.41, 151.57, 141.94, 137.11, 136.71, 133.47, 129.50, 128.55, 127.34, 125.85, 125.77, 124.07, 122.84, 122.10, 121.98, 120.96, 113.80, 111.80, 109.38, 104.92, 37.62; HRMS Calcd for $C_{28}H_{23}N_3O_3S_2$ $(M+H)^+$ 506.0808, found 506.0806.

(*E*)-*N*-(2,6-difluorophenyl)-2-((6-(((2-hydroxynaphthalen-1-yl)methylene)amino)benzo[*d*]thiazol-2-yl)thio)acetamide (ZBTI09): Orange solid; Yield: 85 %; MP: 202-204 ˚C; R_f: 0.78 in 30 % ethyl acetate-*n*-hexane; FTIR (KBr, *v,* cm^{-1}): 3432 (O-H str), 3253 (N-H str), 2922 (aromatic C-H str), 1675 (C=N str), 1622 (C=O str), 1534 (aromatic C=C str) 1022 (aromatic C-F str); ^{1}H NMR (500 MHz, DMSO-d_6) δ 15.71 (s, 1H), 10.22 (s, 1H), 9.77 (s, 1H), 8.56 (s, 1H), 8.39 (d, J = 2.3 Hz, 1H), 7.96 (d, J = 9.2 Hz, 1H), 7.92 (d, J = 8.5 Hz, 1H), 7.83 (d, J = 6.4 Hz, 1H), 7.78 – 7.72 (m, 1H), 7.57 (t, J = 8.5 Hz, 1H), 7.38 (t, J = 7.5 Hz, 2H), 7.18 (t, J = 8.2 Hz, 2H), 7.07 (d, J = 9.2 Hz, 1H), 4.46 (s, 2H); ^{13}C NMR (126 MHz, DMSO-d_6) δ 169.28, 166.48, 166.24, 159.14, 157.16, 156.99, 151.61, 141.92, 137.11, 136.74, 133.48, 129.50, 128.71, 128.56, 127.35, 124.08, 122.11, 121.99, 120.97, 114.62, 113.77, 112.48, 112.29, 109.39, 36.94; HRMS Calcd for $C_{26}H_{17}F_2N_3O_2S_2$ $(M+H)^+$ 506.0808, found 506.0814.

(*E*)-*N*-(2,3-dichlorophenyl)-2-((6-(((2-hydroxynaphthalen-1-yl)methylene)amino)benzo[*d*]thiazol-2-yl)thio)acetamide (ZBTI10): Brick red solid; Yield: 73 %; MP: 209-211 ˚C; R_f: 0.60 in 30 % ethyl acetate-*n*-hexane; FTIR (KBr, *v,* cm^{-1}): 3438 (O-H str), 3259 (N-H str), 2922 (aromatic C-H str), 1700 (C=N str), 1621 (C=O str), 1522 (C=C str), 740 (aromatic C-Cl str); ^{1}H NMR (500 MHz, DMSO-d_6) δ 15.71 (s, 1H), 10.17 (s, 1H), 9.78 (s, 1H), 8.55 (d, J = 8.2 Hz, 1H), 8.39 (d, J = 2.3 Hz, 1H), 7.95 (dd, J = 19.9, 8.9 Hz, 2H), 7.84 (d, J = 8.1 Hz, 1H), 7.79 – 7.74 (m, 2H), 7.58 (t, J = 7.7 Hz, 1H), 7.49 (d, J = 8.1 Hz, 1H), 7.38 (t, J = 8.1 Hz, 2H), 7.08 (d, J = 9.2 Hz, 1H), 4.49 (s, 2H); ^{13}C NMR (126 MHz, DMSO) δ 166.67, 151.54, 142.01, 137.13, 128.63, 128.58, 127.36, 122.16, 121.98, 120.99, 113.92, 109.40, 37.57; HRMS Calcd for $C_{26}H_{17}Cl_2N_3O_2S_2$ $(M+H)^+$ 538.0217, found 538.0217.

(*E*)-*N*-(3,4-dichlorophenyl)-2-((6-(((2-hydroxynaphthalen-1-yl)methylene)amino)benzo[*d*]thiazol-2-yl)thio)acetamide (ZBTI11): Light orange solid; Yield: 78 %; MP: 207-209 ˚C; R_f: 0.66 in 30 % ethyl acetate-*n*-hexane; FTIR (KBr, *v,* cm^{-1}): 3437 (O-H str), 3244 (N-H str), 3086 (aromatic C-H str), 1696 (C=N str), 1621 (C=O str), 1543 (aromatic C=C str), 749 (aromatic C-Cl); ^{1}H NMR (500 MHz, DMSO-d_6) δ 15.69 (s, 1H), 10.76 (s, 1H), 9.76 (s, 1H), 8.54 (d, J = 8.4 Hz, 1H), 8.38 (d, J = 2.3 Hz, 1H), 8.03 – 7.94 (m, 2H), 7.89 (d, J = 8.7 Hz, 1H), 7.83 (d, J = 6.7 Hz, 1H), 7.73 (d, J = 11.0 Hz, 1H), 7.64 – 7.55 (m, 2H), 7.54 – 7.50 (m, 1H), 7.38 (t, J = 7.4 Hz, 1H), 7.07 (d, J = 9.2 Hz, 1H), 4.44 (s, 2H); ^{13}C NMR (126 MHz, DMSO-d_6) δ 169.24, 166.55, 166.29, 157.02, 151.56, 141.98, 139.29, 137.12, 136.70, 133.46, 131.60, 131.33, 129.51, 128.57, 127.35, 125.60, 124.08, 122.14, 121.97, 120.97, 120.86, 119.74, 113.85, 109.39, 38.22; HRMS Calcd for $C_{26}H_{17}Cl_2N_3O_2S_2$ $(M+H)^+$ 538.0217, found 538.0240.

(*E*)-*N*-(2,4-dichlorophenyl)-2-((6-(((2-hydroxynaphthalen-1-yl)methylene)amino)benzo[*d*]thiazol-2-yl)thio)acetamide (ZBTI12): Dark orange solid; Yield: 68 %; MP: 201-203 ˚C; R_f: 0.91 in 30 % ethyl acetate-*n*-hexane; FTIR (KBr, *v,* cm^{-1}): 3437 (O-H str), 3268 (N-H str), 2992 (aromatic C-H str), 1658 (C=N str), 1622 (C=O str), 1521 (aromatic C=C str), 748 (aromatic C-Cl str); ^{1}H NMR (500 MHz, DMSO-d_6) δ 15.71 (s, 1H), 10.10 (s, 1H), 9.74 (d, J = 18.6 Hz, 1H), 8.54 (t, J = 8.7 Hz, 1H), 8.39 (s, 1H), 7.97 (d, J = 9.2 Hz, 1H), 7.92 (d, J = 8.7 Hz, 1H), 7.83 (dd, J = 8.4, 4.7 Hz, 2H), 7.75 (dd, J = 8.7, 2.3 Hz, 1H), 7.69 (d, J = 2.6 Hz, 1H), 7.57 (t, J = 7.8 Hz, 1H), 7.44 (d, J = 8.7 Hz, 1H), 7.38 (t, J = 7.4 Hz, 1H), 7.08 (d, J = 9.2 Hz, 1H), 4.48 (s, 2H). ^{13}C NMR (126 MHz, DMSO-d_6) δ 169.31, 166.67, 151.53, 141.94, 139.33, 136.96, 136.74, 134.26, 133.47, 129.83, 129.59, 129.49, 128.21, 128.12, 127.34, 127.03, 122.22, 122.04, 121.02, 113.92, 113.79, 109.39, 37.76; HRMS Calcd for $C_{26}H_{17}Cl_2N_3O_2S_2$ $(M+H)^+$ 538.0217, found 538.0229.

(*E*)-*N*-(3,4-dimethylphenyl)-2-((6-(((2-hydroxynaphthalen-1-yl)methylene)amino)benzo[*d*]thiazol-2-yl)thio)acetamide (ZBTI13): Dark orange solid; Yield: 77 %; MP: 149-151 ˚C; R_f: 0.78 in 30 % ethyl acetate-*n*-hexane; FTIR (KBr, *v,* cm^{-1}): 3434 (O-H str), 3254 (N-H str), 3065 (aromatic C-H str), 1686 (C=N str), 1619 (C=O str), 1543 (aromatic C=C str); ^{1}H NMR (500 MHz, DMSO-d_6) δ 15.70 (d, J = 4.0 Hz, 1H), 10.28 (s, 1H), 9.77 (s, 1H), 8.54 (d, J = 8.5 Hz, 1H), 8.38 (s, 1H), 7.97 (d, J = 9.2 Hz, 1H), 7.91 (d, J = 8.7 Hz, 1H), 7.83 (d, J = 9.3 Hz, 1H), 7.74 (d, J = 8.7 Hz, 1H), 7.60 – 7.55 (m, 1H), 7.42 – 7.36 (m, 2H), 7.32 (d, J = 8.1 Hz, 1H), 7.07 (d, J = 9.2 Hz, 2H), 4.39 (s, 2H), 2.19 (d, J = 12.1 Hz, 6H); HRMS Calcd for $C_{28}H_{23}N_3O_2S_2$ $(M+H)^+$ 498.1310, found 498.1341; HPLC purity: 98.36 %.

(*E*)-*N*-(2,6-dimethylphenyl)-2-((6-(((2-hydroxynaphthalen-1-yl)methylene)amino)benzo[*d*]thiazol-2-yl)thio)acetamide (ZBTI14): Orange solid; Yield: 81 %; MP: 206-208 ˚C; R_f: 0.74 in 30 % ethyl acetate-*n*-hexane; FTIR (KBr, *v,* cm^{-1}): 3330 (O-H str), 3213 (N-H str), 2922 (aromatic C-H str), 1691 (C=N str), 1621 (C=O str), 1544 (aromatic C=C str); ^{1}H NMR (500 MHz, $CDCl_3$) δ 15.28 (s, 1H), 9.49 (s, 1H), 8.87 (s, 1H), 8.19 (d, J = 8.4 Hz, 1H), 7.90 (dd, J = 23.6, 8.9 Hz, 2H), 7.82 – 7.74 (m, 2H), 7.57 (t, J = 7.0 Hz, 1H), 7.49 (d, J = 8.7 Hz, 1H), 7.40 (t, J = 6.9 Hz, 1H), 7.18 (d, J = 9.2 Hz, 1H), 7.14 – 7.06 (m, 3H), 4.22 (s, 2H), 2.21 (s, 6H); ^{13}C NMR (126 MHz, $CDCl_3$) δ 167.49, 166.91, 166.67, 156.60, 150.86, 144.06, 136.96, 136.47, 135.29, 133.63, 132.99, 129.47, 128.26, 128.19, 127.64, 127.39, 123.78, 122.10, 121.14, 120.14, 119.07, 112.97, 109.27, 36.22, 18.30; HRMS Calcd for $C_{28}H_{23}N_3O_2S_2$ $(M+H)^+$ 498.1310, found 498.1360; HPLC purity: 97.89 %.

2.8. Biological studies

2.8.1. *In vitro* studies

The multitarget inhibition profile of compounds **ZBTI01-ZBTI14** was evaluated against monoamine oxidases (MAO-A and MAO-B) and cholinesterases (AChE and BChE) through the peroxidase-linked colorimetric method and Ellman's UV-based spectrophotometric method, respectively. The obtained enzyme inhibition results (IC_{50}) of all the test and reference inhibitors along with their selectivity index against MAO-B are provided in **Table 2.3.**

Table 2.3. *In vitro* enzyme inhibition results of compounds **ZBTI01-ZBTI14**

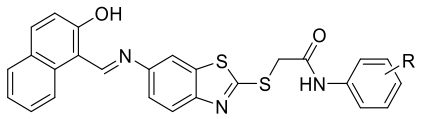

ZBTI01-ZBTI14

Compound code	R	MAO-A IC_{50} (µM)[a]	MAO-B IC_{50} (µM)[a]	AChE IC_{50} (µM)[b]	BChE IC_{50} (µM)[b]	S.I.[c]
ZBTI01	H	0.464 ± 0.067	0.971 ± 0.041	0.188 ± 0.064	NT	0.48
ZBTI02	4-F	0.047 ± 0.019	0.246 ± 0.014	0.148 ± 0.008	NT	0.19
ZBTI03	4-Cl	0.315 ± 0.002	0.138 ± 0.034	0.156 ± 0.003	NT	2.28
ZBTI04	4-Br	0.076 ± 0.004	0.317 ± 0.001	0.178 ± 0.068	NT	0.24
ZBTI05	4-CH_3	0.100 ±0.013	0.099 ± 0.014	0.170 ± 0.006	NT	1.01
ZBTI06	4-OCH_3	0.626 ± 0.092	1.110 ± 0.059	0.133 ± 0.012	NT	0.56
ZBTI07	4-OC_2H_5	1.060 ± 0.153	0.070 ± 0.016	0.150 ± 0.019	NT	15.14
ZBTI08	2,4-F_2	0.120 ± 0.004	0.260 ± 0.045	0.147 ± 0.015	NT	0.46
ZBTI09	2,6-F_2	0.287 ± 0.030	3.214 ± 0.094	0.148 ± 0.019	NT	0.09
ZBTI10	2,3-Cl_2	0.220 ± 0.033	1.315 ± 0.226	0.143 ± 0.013	NT	0.17
ZBTI11	3,4-Cl_2	0.030 ± 0.008	2.557 ± 0.583	0.139 ± 0.013	NT	0.01
ZBTI12	2,4-Cl_2	0.419 ± 0.040	0.088 ± 0.006	0.186 ± 0.064	NT	4.76
ZBTI13	3,4-$(CH_3)_2$	1.400 ± 0.094	0.015 ± 0.007	0.114 ± 0.003	4.125 ± 0.143	93.33
ZBTI14	2,6-$(CH_3)_2$	1.931 ± 0.092	0.060 ± 0.007	0.119 ± 0.002	NT	32.18
CLO	-	0.096 ± 0.003	-	-	-	-
SEL	-	-	0.021 ± 0.002	-	-	-

PCPA	-	0.141 ± 0.002	0.201 ± 0.001	-	-	0.70
DPZ	-	-	-	0.068 ± 0.009	1.751 ± 0.120	-

[a] Mean IC_{50} (μM) ± SEM of 2 independent experiments in triplicate; [b] Values are the mean ± SEM of 3 independent experiments in triplicate; [c] Selectivity index: ratio of experimental IC_{50} (MAO-A)/IC_{50} (MAO-B); CLO = Clorgyline, SEL = Selegiline, PCPA = Tranylcypromine; NT = Not tested.

2.8.1.1. *In vitro* MAO inhibition studies

The enzyme inhibition results (IC_{50}) of compounds **ZBTI01-ZBTI14** against MAO-A were obtained in the range of micromolar to nanomolar concentration (1.931 ± 0.092 μM to 0.030 ± 0.008 μM) and listed in **Table 2.3**. The obtained IC_{50} values against MAO-A ranged from 1.931 ± 0.092 μM (compound **ZBTI14**) to 0.030 ± 0.008 μM (compound **ZBTI11**). Compound **ZBTI11** was identified as the most potent MAO-A inhibitor with IC_{50} value 0.030 ± 0.008 μM. The compounds **ZBTI01-ZBTI14** were also screened against MAO-B and the obtained results ranged from micromolar to nanomolar concentration (3.214 ± 0.094 to 0.015 ± 0.007 μM) and are given in **Table 2.3**. Compound **ZBTI13**) was identified as the most potent MAO-B inhibitor with an IC_{50} value of 0.015 ± 0.007 μM.

SAR of MAO-A-inhibition

- Most of the tested compounds showed IC_{50} values lower than 1 μM (except compounds **ZBTI07**, **ZBTI13** and **ZBTI14**). Among the tested compounds, analog with 3,4-dichloro substitution (compound **ZBTI11**) was identified as the most potent MAO-A inhibitor with an IC_{50} value of 0.030 ± 0.008 μM and was more potent than the reference inhibitor, clorgyline.
- Introduction of a halogen atom at the 4^{th} position of the phenyl ring (compounds **ZBTI02- ZBTI04**) particularly with a fluorine (compound **ZBTI02**) or bromine (compound **ZBTI04**) atom significantly enhanced the MAO-A inhibition activity (~10-fold and ~6-fold, respectively) compared to the unsubstituted parent compound **ZBTI01**.

- On the other hand, enriching the phenyl ring with two fluorine atoms produced relatively less potent analogs (compounds **ZBTI07** and **ZBTI08**) compared to the mono-fluoro analog (compound **ZBTI02**).
- Similarly, enriching the phenyl ring with two chloro groups produced more potent analogs (compounds **ZBTI10** and **ZBTI11**, except compound **ZBTI12**) and especially the 3,4-dichloro substituted analog was ~10-fold more potent than the mono-chloro analog (compound **ZBTI03**).
- Substitution with 4-methyl group (compound **ZBTI05**) increased MAO-A inhibition activity by ~4-fold while 4-methoxyl (compound **ZBTI06**) and 4-ethoxyl (compound **ZBTI07**) drastically decreased the MAO-A inhibition activity.
- The introduction of the 4-methyl group (compound **ZBTI05**) on the aryl ring slightly enhanced the MAO activity (compared to parent analog **ZBTI01**) however, the inclusion of dimethyl groups (3,4-dimethyl and 2,6-dimethyl in compound **ZBTI13** and **ZBTI14**, respectively) resulted in a drastic reduction in MAO-A inhibitory activity.
- Overall, the presence of less bulky substituent on the phenyl ring favored MAO-A inhibitory activity whereas the presence of steric or bulky groups such as 4-methoxy (compound **ZBTI06**), 4-ethoxy (compound **ZBTI07**), 3,4-dimethyl (compound **ZBTI13**) and 2,6-dimethyl (compound **ZBTI14**) decreased the MAO-A inhibitory activity.

SAR of MAO-B inhibition

- The compounds **ZBTI01-ZBTI14** were screened against MAO-B and the obtained results ranged from micromolar to nanomolar concentration (3.214 ± 0.094 to 0.015 ± 0.007 μM) and are given in **Table 2.3**.

- Analog with 3,4-dimethyl substitution (compound **ZBTI13**) emerged as the most potent MAO-B inhibitor with an IC_{50} value of 0.015 ± 0.007 μM, more potent than reference inhibitor selegiline. While analog with 2,6-dimethyl substitution (**ZBTI14**) was identified as the second most potent MAO-B inhibitor with an IC_{50} value of 0.060 ± 0.007 μM.

- Most of the compounds displayed IC_{50} less than 1 μM except compounds **ZBTI06**, **ZBTI09**, **ZBTI10** and **ZBTI11**.

- Analogs mono-substituted with 4-fluoro (compound **ZBTI02**), 4-chloro (compound **ZBTI03**), 4-bromo (compound **ZBTI04**) and 4-methyl (compound **ZBTI05**) resulted in enhanced MAO-B inhibitory activity than unsubstituted parent analog (compound **ZBTI01**).

- The introduction of the di-fluoro group at 2,4-difluoro (compound **ZBTI08**) slightly reduced the activity but substitution with 2,6-difluoro group drastically reduced MAO-B inhibitory activity of resulting analog (compound **ZBTI09**) than mono substituted analog (compound **ZBTI01**).

- Changing lipophilicity of the 4-methyl group (compound **ZBTI05**) with a 4-methoxyl group (compound **ZBTI06**) reduced (~11-fold) activity while the 4-ethoxyl group (compound **ZBTI07**) increased MAO-B inhibitory activity.

- Substitution of additional chloro group on N-terminal aryl ring with 2,3-dichloro (compound **ZBTI10**), and 3,4-dichloro (compound **ZBTI11**) displayed drastic loss of MAO-B inhibitory activity by ~10-fold and ~19-fold, respectively, (compare with compound **ZBTI03**) but introduction of 2,4-dichloro resulted in an increase of ~1.5-fold in MAO-B inhibitory potency.

2.8.2. *In vitro* ChEs inhibition studies

The compounds **ZBTI01-ZBTI14** were screened against *ee*AChE while compound **ZBTI13** was also evaluated against *eq*BChE to check the selectivity between AChE & BChE and the recorded IC_{50} values are listed in **Table 2.3.** The obtained IC_{50} values were in submicromolar range from 0.188 ± 0.064 μM (compound **ZBTI01**) to 0.114 ± 0.003 μM (compound **ZBTI13**). Compound **ZBTI13** was identified as the most potent molecule among all the tested compounds with an IC_{50} value of 0.114 ± 0.003 μM.

SAR of AChE inhibition

- Compounds **ZBTI01-ZBTI14** were screened against *ee*AChE and recorded IC_{50} values lie in (a narrow) submicromolar range (0.114 ± 0.003 μM to 0.188 ± 0.064 μM) as listed in **Table 2.3**.
- Analogs with di-methyl substitution (compounds **ZBTI13** and **ZBTI14**) emerged as the most potent inhibitors of AChE among all the tested compounds.
- Introduction of mono substituent with 4-fluoro (compound **ZBTI02**), displayed slightly increased AChE inhibition while di-substitution with 2,4-difluoro (compound **ZBTI07**), 2,6-difluoro (compound **ZBTI08**) caused no change in the activity.
- Analog with 4-chloro substitution (compound **ZBTI03**) showed mild activity towards AChE than unsubstituted parent analog (compound **ZBTI01**) while placement of additional chloro group at 2,3-dichloro (compound **ZBTI10**), 3,4-dichloro (compound **ZBTI11**) increased AChE inhibition but 2,4-dichloro (compound **ZBTI12**) substitution led to reduction in AChE inhibitory activity.
- Substitution with the 4-bromo (compound **ZBTI04**) group moderately enhanced AChE inhibition of the resulting analog.

- Replacement of 4-methyl (compound **ZBTI05**) with 4-methoxyl (compound **ZBTI06**) and 4-ethoxyl (compound **ZBTI07**) moderately increased AChE inhibition of resulting analogs.
- All the compounds exhibited IC_{50} less than 0.2 µM.

2.8.2.1. Enzyme kinetics and reversibility

A double reciprocal plot was constructed to determine the type of enzyme inhibition by compound **ZBTI13** against MAO-B and AChE. Analysis of double reciprocal plots indicates competitive and mixed type of inhibition of MAO-B and AChE enzymes by compound **ZBTI13**, respectively (**Figure 2.11A** & **2.11D**). The examination of the time-dependent reversibility study revealed the reversible type of inhibition of both enzymes by compound **ZBTI13** (**Figure 2.11C** & **2.11F**). Further, a Dixon plot was constructed to determine the experimental Ki value of compound **ZBTI13** against both target enzymes. The obtained Ki values for MAO-B was 41.99 µM and for AChE, it was 33.25 µM.

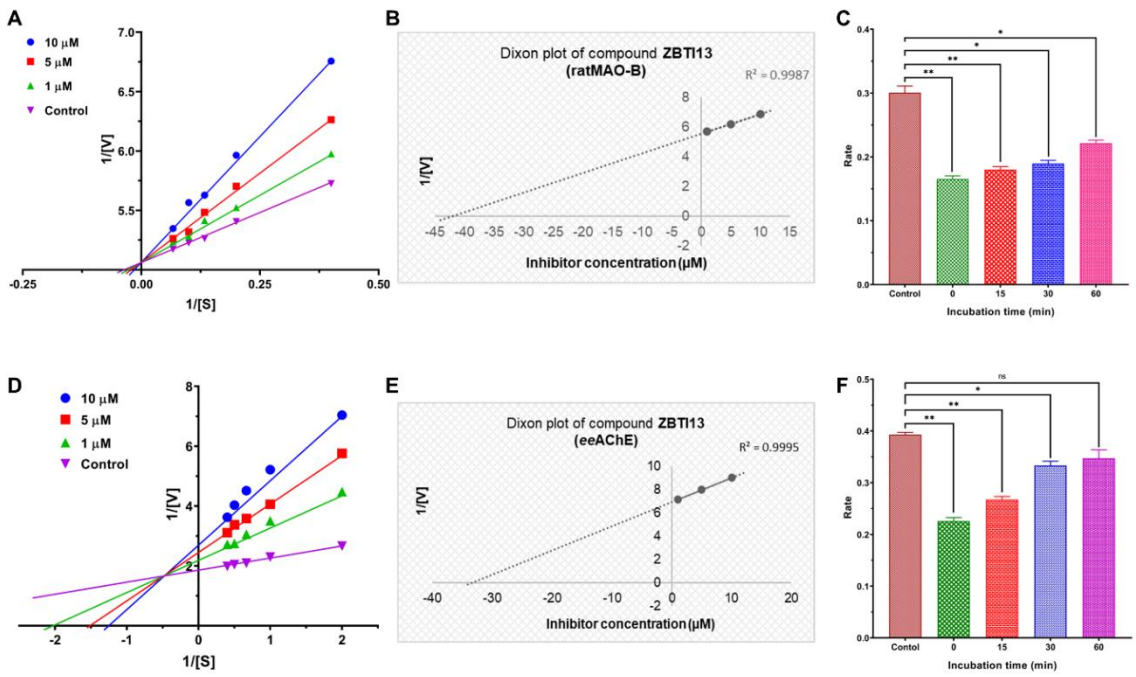

Figure 2.11. Enzyme kinetics, time-dependent reversibility study and Dixon plot of compound **ZBTI13** with MAO-B and AChE; A) Enzyme kinetics graph of compound

ZBTI13 with MAO-B; B) Dixon plot of compound **ZBTI13** with MAO-B; C) Time-dependent reversibility graph of compound **ZBTI13** with MAO-B enzyme; D) Enzyme kinetics graph of compound **ZBTI13** with AChE; E) Dixon plot of compound **ZBTI13** with AChE; F) Time-dependent reversibility graph of compound **ZBTI13** with AChE enzyme.

2.8.2.2. *In vitro* antioxidant assay

Selected compounds **ZBTI02**, **ZBTI03-ZBTI07** and **ZBTI10-ZBTI14** along with marketed drug molecules donepezil (DPZ), selegiline (SEL), tranylcypromine (PCPA) were used for antioxidant evaluation through 2,2-diphenyl-1-picrylhydrazyl (DPPH assay) method. Ascorbic acid (AA) was used as the reference antioxidant drug. The graph of % FRS is presented in **Figure 2.12** whereas EC_{50} values are mentioned in **Table 2.4**. From the % FRS graph we can conclude that compound **ZBTI04** has shown the most potency towards the free radical scavenging.

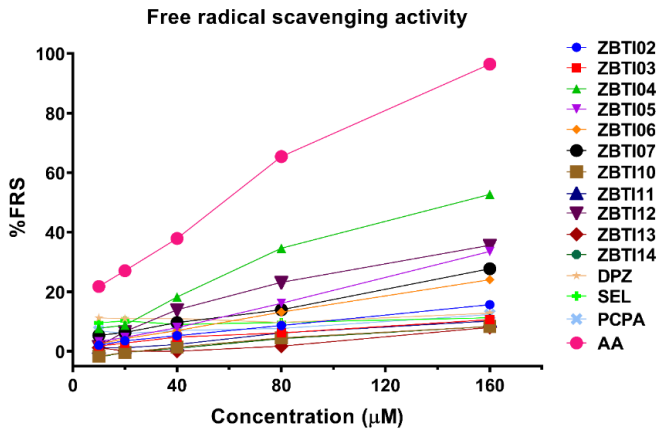

Figure 2.12. Free radical scavenging activity of selected compounds

Some of the tested compounds (**ZBTI04**, **ZBTI05** and **ZBTI12**) displayed moderate free radical activity against DPPH while other test compounds and marketed drugs showed weak antioxidant activity as compared to reference drug ascorbic acid (**Table 2.4**).

Table 2.4. Antioxidant activity % FRS of selected compounds

Compound code	Antioxidant activity by DPPH assay	
	% FRS[a]	EC_{50} (μM)
ZBTI02	19.28 ± 0.484	557.62 ± 19.48
ZBTI03	13.07 ± 1.100	930.08 ± 40.83
ZBTI04	67.22 ± 0.366	144.93 ± 2.36
ZBTI05	41.30 ± 0.003	244.10 ± 3.23
ZBTI06	29.98 ± 0.056	335.93 ± 7.16
ZBTI07	33.15 ± 0.164	292.83 ± 18.90
ZBTI10	11.50 ± 0.148	736.22 ± 3.13
ZBTI11	13.28 ± 0.293	760.14 ± 23.57
ZBTI12	46.24 ± 0.433	214.41 ± 4.37
ZBTI13	8.35 ± 0.783	1162.87 ± 52.24
ZBTI14	11.57 ± 0.077	720.47 ± 12.62
Donepezil	11.70 ± 0.810	2174.10 ± 79.56
Selegiline	11.26 ± 0.150	1613.30 ± 46.04
Tranylcypromine	12.68 ± 0.736	1324.80 ± 40.54
Ascorbic acid[b]	66.89 ± 2.070	62.14 ± 0.36

[a] % FRS at a concentration of 200 μM; [b] % FRS at a concentration of 100 μM.

2.8.2.3. *In vitro* metal chelation assay

Selected compounds (compounds **ZBTI11**, **ZBTI13** and **ZBTI14**) were selected for iron chelation properties using a UV-vis-based method. Ferric chloride hexahydrate was used as the iron source while 8-hydroxyquinoline was used as reference iron chelator. Peak shift of absorption maxima (λ) due to chelation of iron can be seen in the graph of each compound and reference molecule (**Figure 2.13**).

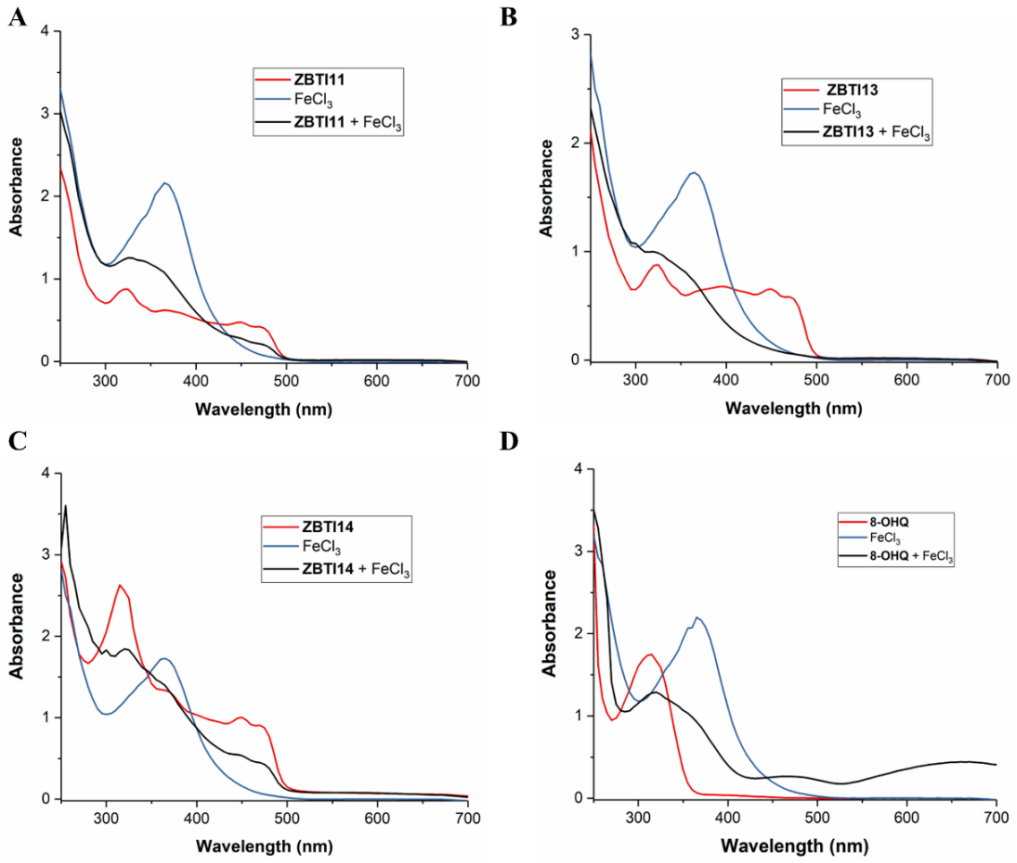

Figure 2.13. UV absorption spectra of compounds **ZBTI11**, **ZBTI13** and **ZBTI14** alone and with $FeCl_3$; A) Compound **ZBTI11**; B) Compound **ZBTI13**; C) Compound **ZBTI14** and D**) 8-OHQ** (8-Hydroxyquinoline) as reference iron chelator.

2.8.2.4. *In vitro* blood-brain-barrier permeation assay

PAMPA-BBB is a permeability assay based on the passive permeation of the compound through an artificial membrane porcine brain lipid (PBL) coated filter membrane and mimics the actual blood-brain barrier [178]. Each brain targeting molecule must often cross the BBB to reach and exhibit its therapeutic effect in the brain. Parallel Artificial Membrane Permeability Assay (PAMPA) is a fast and less expensive high-throughput screening method for permeability evaluation of test compounds. As our compound **ZBTI13** targets enzymes in the brain, the compound was assessed for its *in vitro* blood-brain-barrier permeability. Selegiline and donepezil were used as reference standards while imipramine & tenoxicam were used as positive and negative permeability controls, respectively. **Table 2.5** shows the effective permeability (P_e) values of tested molecules. The effective

permeability (P_e) value of (3.154 ± 0.204) ×10^{-6} cm/s was obtained for compound **ZBTI13** after 18 h of incubation. As per Di *et al.*, any molecule is considered a CNS+ molecule if it has $P_e > 4.0 \times 10^{-6}$ cm/s, is CNS± if it has $Pe > 2.0 \times 10^{-6}$ cm/s and $< 4.0 \times 10^{-6}$ cm/s and is CNS- when $P_e < 2.0 \times 10^{-6}$ cm/s. The obtained results indicate ambiguous CNS permeability i.e., compound **ZBTI13** may or may not passively diffuse to the brain through BBB.

Table 2.5. PAMPA assay data for compound **ZBTI13**

Compound ID	P_e (x10^{-6} cm/s)[a]	Reference P_e (x10^{-6} cm/s)[b]	*In Silico* Predicted BBB permeability[c]	CNS Category[d]	Literature CNS category[b]
ZBTI13	3.154 ± 0.204	NA	0.057	CNS±	NA
Donepezil	7.504 ± 0.305	6.80	0.188	CNS+	CNS+
Selegiline	6.417 ± 0.205	5.69	4.435	CNS+	CNS+
Imipramine[e]	14.922 ± 0.131	13	2.920	CNS+	CNS+
Tenoxicam[e]	1.267 ± 0.168	0.1	0.095	CNS-	CNS-

[a] P_e values as mean ± SD of two independent experiments in duplicate.
[b] Values are cited from Di *et.al.*, 2003.
[c] BBB permeability using PreADMET web-based server (accessed on 08.08.2024).
[d] CNS+ ($P_e > 4.0 \times 10^{-6}$ cm/s), CNS± ($P_e > 2.0 \times 10^{-6}$ cm/s $< 4.0 \times 10^{-6}$ cm/s), CNS- ($P_e < 2.0 \times 10^{-6}$ cm/s)[b]
[e] Used as positive and negative permeability controls respectively.

2.8.2.5. Cell-based toxicity assay

The compound **ZBTI13** was investigated for its cytotoxicity in fibroblast cells (L929) and neurotoxicity using neuroblastoma cell lines (SH-SY5Y) using MTT assay (**Figure 2.14**). The cells were treated with different concentrations (0.1, 1, 10 50 and 100 µM) of compound **ZBTI13** for 24 h followed by MTT assay. The obtained results indicate that compound **ZBTI13** was non-toxic up to 10 µM concentration in fibroblast cells and up to 50 µM concentration in the neuroblastoma cell lines above which cytotoxicity (L929) and neurotoxicity (SH-SY5Y) was observed. The percent cell viability graph versus concentration plot of compound **ZBTI13** against L929 cells is indicated in **Figure 2.15A** while for SH-SY5Y the percent viability is given in **Figure 2.15B**. The inverted

microscopic brightfield image and microscopic fluorescence image of fibroblast cells 24 h post-treatment with **ZBTI13** at 0 µM (control) and 50 µM concentration are shown in **Figure 2.14A** & **2.14B**. The inverted microscopic brightfield image of SH-SY5Y cells 24 h post-treatment with compound **ZBTI13** at 0 µM (control) and 50 µM concentration are shown in **Figures 2.14C** & **2.14D**. From the percent cell viability graph, it can be concluded that compound **ZBTI13** was non-toxic to SH-SY5Y cells.

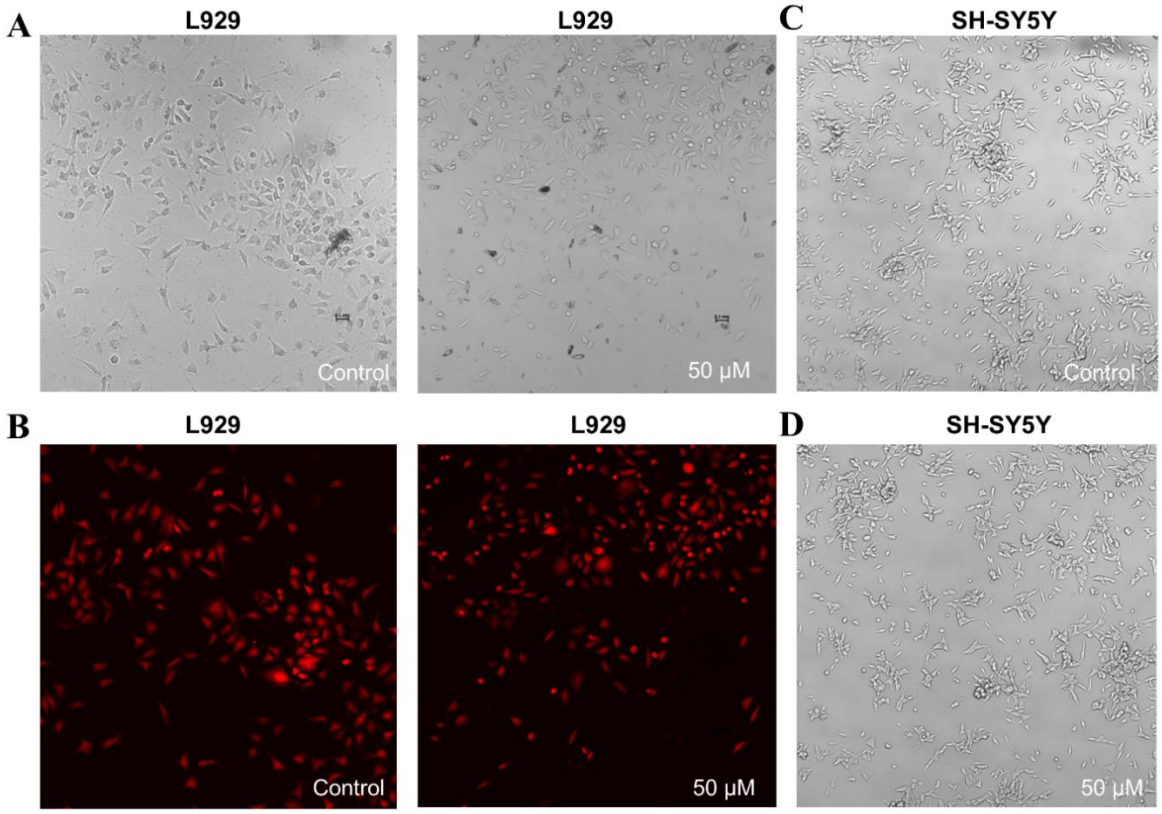

Figure 2.14. *In vitro* toxicity assay of compound **ZBTI13** in fibroblast (L929) and neuroblastoma (SH-SY5Y) cells; A) inverted microscopic brightfield image of L929 cells 24 h post-treatment with compound **ZBTI13** at 0 µM (Control) and 50 µM concentration; B) inverted microscopic fluorescence image of L929 cell 24 h post-treatment with compound **ZBTI13** at 0 µM (Control) and 50 µM concentration; C) microscopic brightfield image of SH-SY5Y cell 24 h post-treatment with compound **ZBTI13** at 0 µM (Control) and D) 50 µM concentration. The images of cells were captured at 10X magnification.

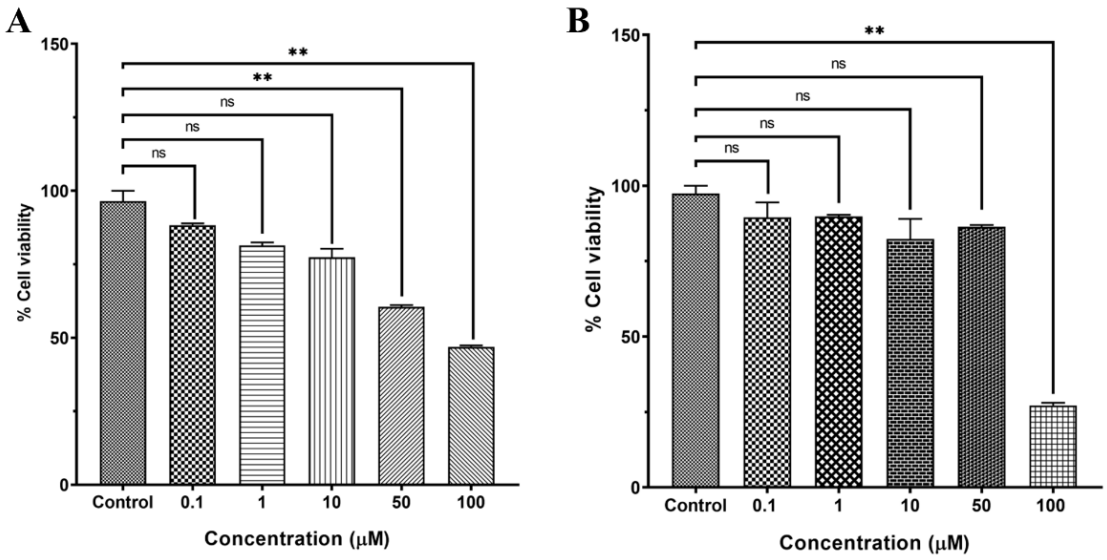

Figure 2.15. Cell viability graphs of compound **ZBTI13** against A) fibroblast (L929); and B) neuroblastoma cell line (SH-SY5Y).

2.8.2.6. Neuroprotection assay using neuroblastoma cell line

After a neurotoxicity study, the compound **ZBTI13** was further evaluated for its neuroprotective potential against dexamethasone-induced oxidative stress in neuroblastoma cell line (SH-SY5Y). Dexamethasone (a cellular stressor) is a fluorinated glucocorticoid that acts through the glucocorticoid receptor (nuclear receptor) in the cell and causes the increase of MAO-B activity in the cells, as well as apoptosis [179, 180]. The cells were loaded into a 96-well cell culture plate and treatment was done with 2 μM of dexamethasone in three different concentrations (0.25, 100 and 200 nM) of test compound **ZBTI13** for 72 h except for control wells (which contained only culture media). The cell survival plot indicates that only the dexamethasone-treated group shows a significant reduction in cell survival while wells-treated with test compound **ZBTI13** displayed significant dose-dependent recovery from oxidative stress caused by dexamethasone. From the graph, it can be concluded that compound **ZBTI13** exhibits its neuroprotective effect against dexamethasone-induced oxidative stress and increased MAO-B levels in the SH-SY5Y cells (**Figure 2.16**).

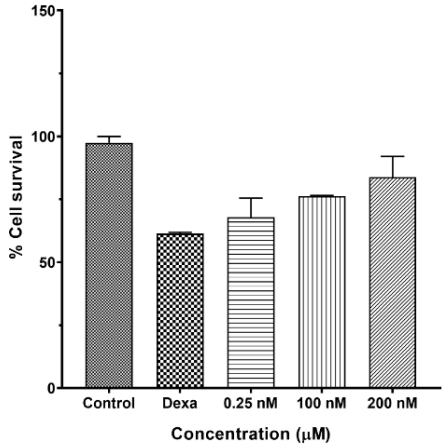

Figure 2.16. *In vitro* neuroprotection assay of compound **ZBTI13** in SH-SY5Y cells against dexamethasone-induced oxidative stress, % cell survival vs. different concentrations (0.25, 100 and 200 nM) of compound **ZBTI13** with 2 μM concentration of dexamethasone.

2.8.3. *In vivo* studies

2.8.3.1. Scopolamine induced amnesia model

The behavioral studies were carried out to evaluate the *in vivo* efficacy of compound **ZBTI13** against the ameliorative potential of cognitive and memory dysfunction in a scopolamine-induced cognition deficit mouse model. Alteration in scopolamine-induced cognitive impairment with the treatment of compound **ZBTI13** was evaluated using the Y-maze test. The spontaneous alternation behavior activity of compound **ZBTI13** (5, 10, and 20 mg/kg) along with the DPZ (5 mg/kg) was determined and obtained (**Figure 2.17**).

2.8.3.2. Y-maze test

Initially, a pilot study was conducted on **ZBTI13** at 5 mg/kg dose to evaluate the *in vivo* efficacy of the compound. Scopolamine-induced amnesia model was used while animal behavior and memory deficit were evaluated using the Y-maze test. Compound **ZBTI13** showed significant improvement in the memory of test animals compared to the scopolamine group. Based on pilot study results, compound **ZBTI13** was further evaluated for dose-dependent effect in the dose of 5, 10 and 20 mg/kg along with donepezil (5 mg/kg), and the percentage of spontaneous alternations was recorded and a graph was plotted. The

results analysis was performed using One-way ANOVA revealed significant differences among the groups. The percentage of alternation was significantly decreased ($p < 0.05$) in the scopolamine (SCO)-treated group compared to the control group, indicating the cognitive impairment induced by scopolamine. A significant increase in % spontaneous alternation was observed in the groups treated with **ZBTI13** (5, 10 and 20 mg/kg) and donepezil, suggesting a reversal of scopolamine-induced deficits. These findings revealed that administration of compound **ZBTI13** at different doses (5, 10 and 20 mg/kg) produced significant improvement in cognitive and memory function in the scopolamine-induced mice model.

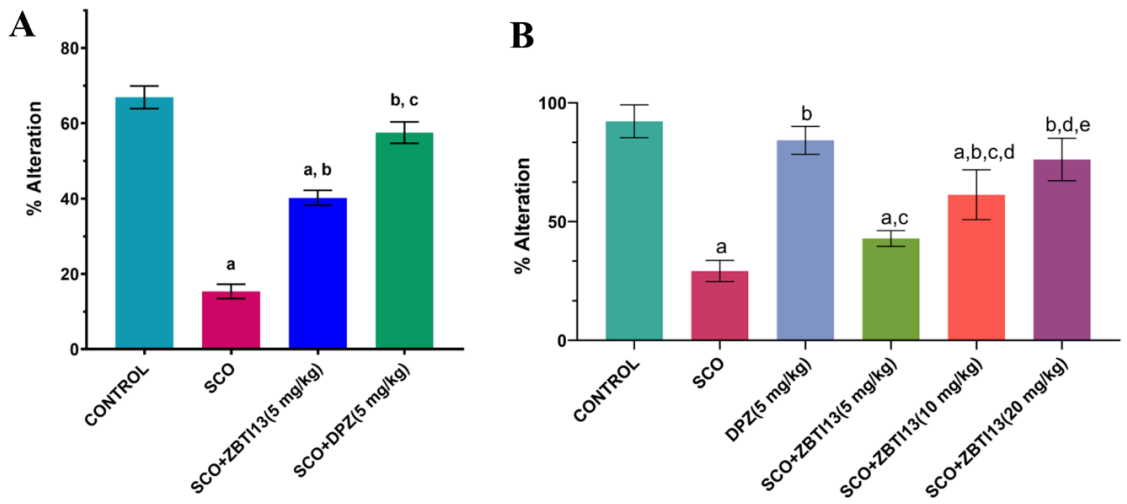

Figure 2.17. Effect of compound **ZBTI13** on scopolamine-induced cognition and memory impairment showing effect on spontaneous alteration A) % $^{a}P < 0.05$ vs. control; $^{b}P < 0.05$ vs. scopolamine; $^{c}P < 0.05$ vs. compound **ZBTI13** (5 mg/kg), $^{d}P < 0.05$ vs. **DPZ** (5 mg/kg); B) Effect of different doses of compound **ZBTI13** on scopolamine-induced cognition and memory impairment showing effect on spontaneous alteration % $^{a}P < 0.05$ vs. control; $^{b}P < 0.05$ vs. scopolamine; $^{c}P < 0.05$ vs. compound **DPZ** (5 mg/kg), $^{d}P < 0.05$ vs. compound **ZBTI13** (5 mg/kg), $^{e}P < 0.05$ vs. compound **ZBTI13** (10 mg/kg), $^{f}P < 0.05$ vs. compound **ZBTI13** (20 mg/kg).

2.8.3.3. *Ex vivo* biochemical analysis

The effect of compound **ZBTI13** on neurochemical levels was accessed through the estimation of enzyme (AChE), neurotransmitter (ACh), and other important biochemical

parameters such as malondialdehyde (MDA) and catalase (CAT). The supernatant from tissue homogenate of the hippocampus region of the brain was used for the estimation of different biochemicals. The results indicate that the level of ACh was decreased while AChE activity was increased in the groups treated with scopolamine as compared to the control group ($p < 0.05$). However, the animal group treated with compound **ZBTI13** displayed a significantly increased level of ACh and a reduced level of AChE compared to scopolamine-treated mice ($p < 0.05$) (**Figure 2.18A**). Furthermore, the antioxidant potential of the compound **ZBTI13** was evaluated by the estimation of oxidative biochemical markers named malondialdehyde (MDA) and catalase (CAT). The results demonstrated that scopolamine-treated mice significantly decreased CAT levels and elevated the MDA levels as compared to the control group ($p < 0.05$) (**Figure 2.18C**). However, the group treated with compound **ZBTI13** attenuated the levels of MDA while remarkably increasing the level of CAT compared to scopolamine-treated mice. The results also disclosed that the CAT levels increased and MDA decreased significantly in the group treated with DPZ ($p < 0.05$) (**Figure 2.18**). Thus, collectively the obtained *ex vivo* biochemical results suggest AChE inhibitory property of compound **ZBTI13** along with antioxidant potential.

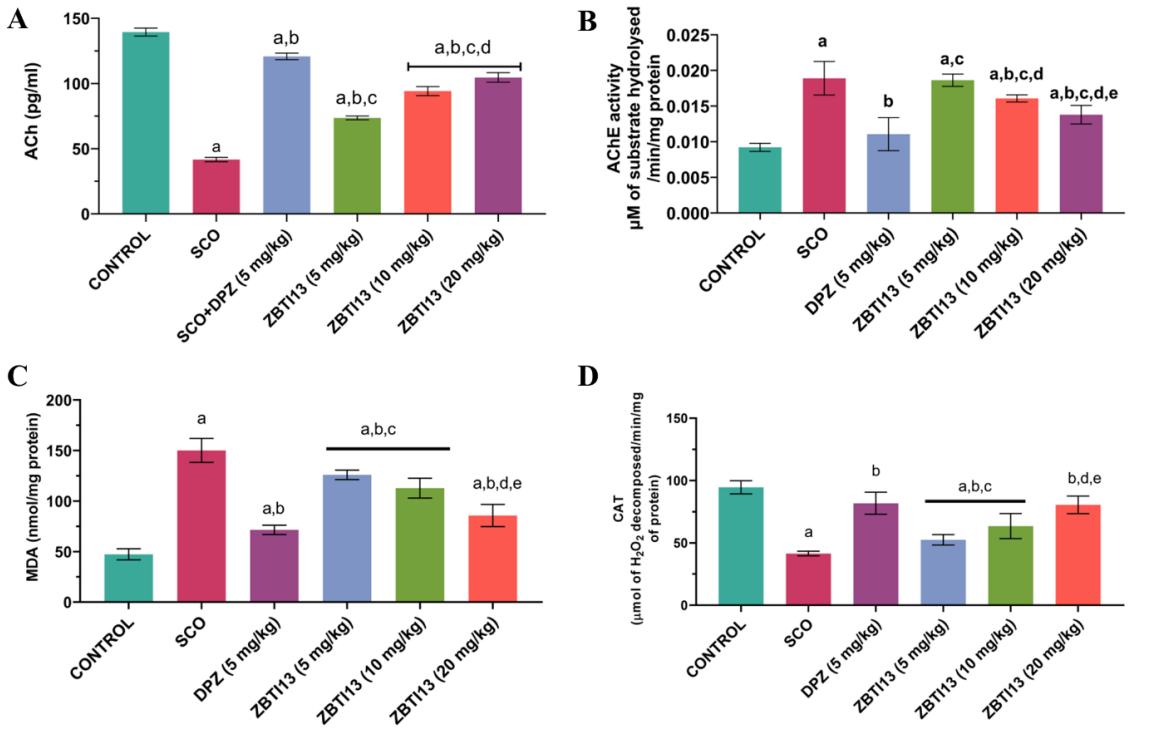

Figure 2.18. Scopolamine-induced memory deficit in mice; (A) Effect of compound **ZBTI13** on the level of ACh; (B) Impact of compound **ZBTI13** on the activity of AChE; (C) Role of compound **ZBTI13** on MDA level and; (D) CAT activity. $^{a}P < 0.05$ vs. control; $^{b}P < 0.05$ vs. scopolamine; $^{c}P < 0.05$ vs. compound **ZBTI13** (5, 10 and 20 mg/kg).

2.8.3.4. *In vivo* acute oral toxicity of compound ZBTI13

According to OECD Guideline 423 (Acute Toxic Class Method) [154], an acute oral toxicity assessment was performed on adult female albino mice to assess *in vivo* safety and ascertain the median lethal dose, or LD_{50}. At the dosage of 300 mg/kg and 2000 mg/kg body weight (BW), no animal was found dead or in a moribund state within 14 days, suggesting that compound **ZBTI13** was safe for all animals, with an LD_{50} of >2000 mg/kg.

At the end of the experiment, the effects of a single oral dose of compound **ZBTI13 (**300 mg/kg and 2000 mg/kg BW) on the organ coefficients of the brain, heart, kidneys, and liver were examined. Animal organ weight is a crucial test parameter in *in vivo* toxicological investigations; variations in the weight of the animal are most important and heavily perfused organs following treatment with a test substance suggest that the organs and vitals may undergo morphological changes that could result in systemic toxicity. An accurate

method of calculating any changes in a test animal's organ weight in relation to changes in its body weight during toxicological studies is to use the organ coefficient. Following animal sacrifice, the impact of a single oral dose of compound **ZBTI13** (300 mg/kg and 2000 mg/kg BW) on the organ coefficients of the crucial organs brain, heart, kidneys, and liver are shown in **Figure 2.19.** Compound **ZBTI13** does not significantly alter the organ coefficient of these highly perfused organs in any of the groups, as shown in the figure. The organ coefficients of the brain, heart, kidneys, and liver did not significantly change among the groups, according to statistical analysis using the one-way ANOVA. We also performed a histopathology analysis as per OECD 423 criteria to look for any tissue damage our test substance might have caused to the aforementioned organs.

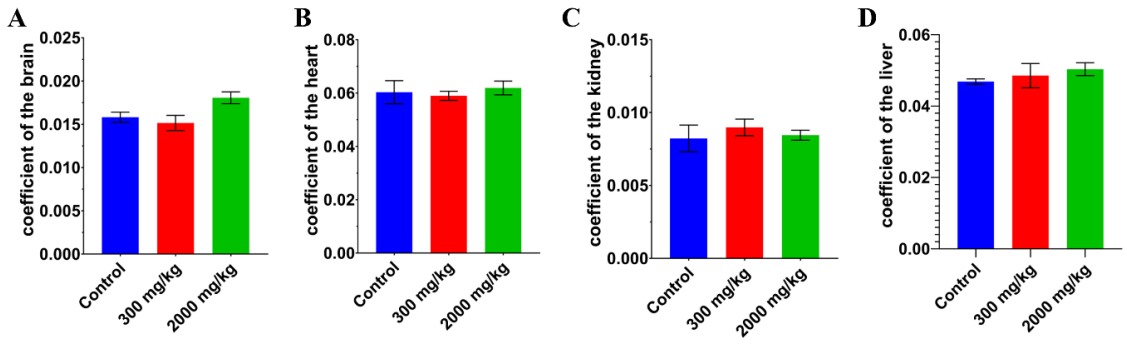

Figure 2.19. Effect of single-dose oral administration of compound **ZBTI13** 300 mg/kg and 2000 mg/kg BW on organ coefficient of the brain, heart, kidneys, and liver at the end of the experiment (14^{th} day).

At the end of the experiment, a single oral administration of a dose of 300 mg/kg and 2000 mg/kg BW of compound **ZBTI13** did not cause any damage to the tissue architecture of the brain, heart, kidneys, and liver; none of these highly perfused organs showed any histopathological changes, as can be seen from the photomicrographs in **Figure 2.20**. Normal brain cortex neurons, normal hepatocytes with acidophilic cytoplasm, intact vesicular nucleus radiating from the central vein surrounding the portal tract, and proper sinusoids in the liver sections were all present. The heart sections also showed normal

myocardial muscle bundles with thin fibro collagenous stroma and at the last normal renal tubules in the kidney sections in all the study groups were observed.

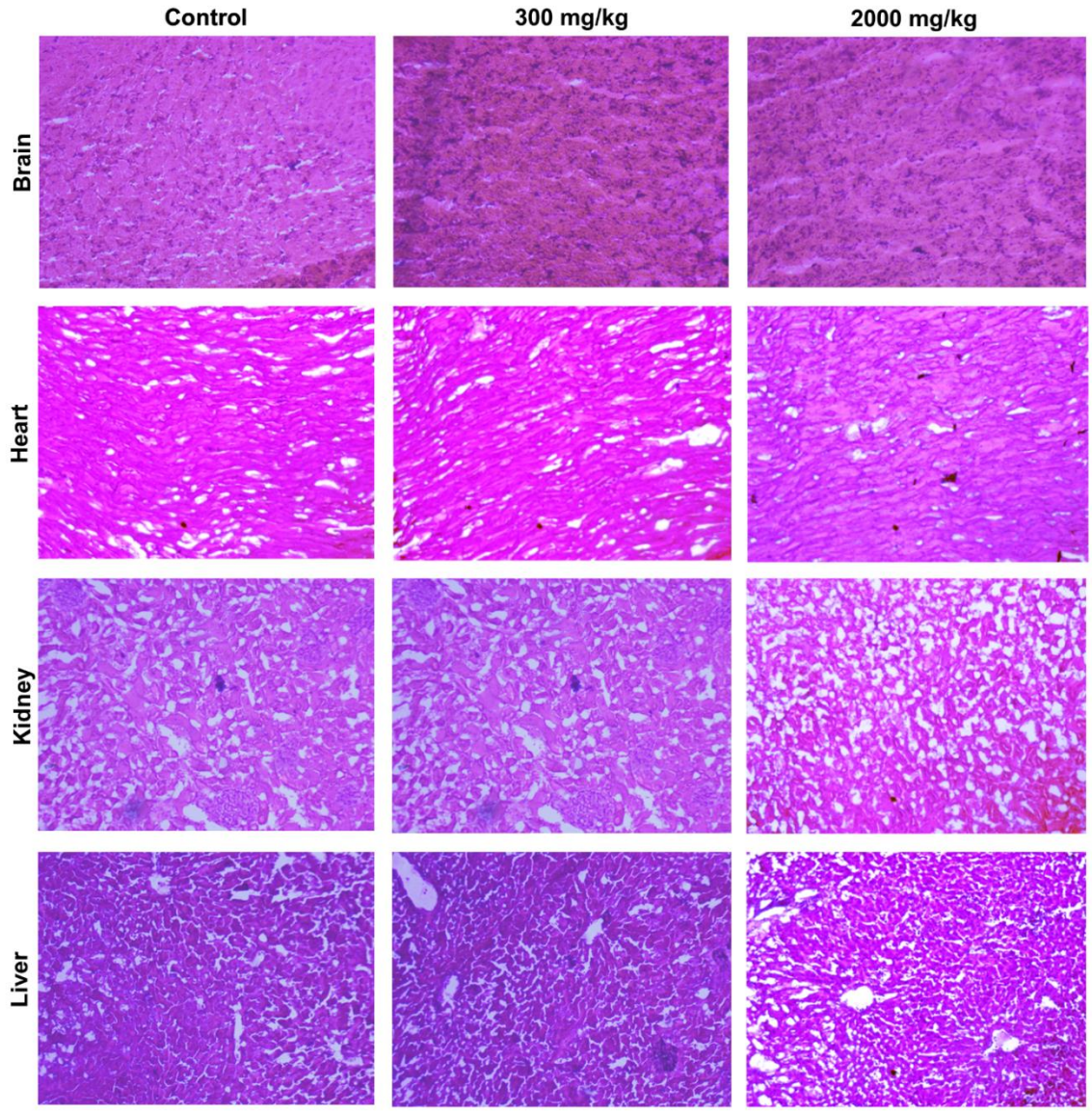

Figure 2.20. Effect of single-dose oral administration of compound **ZBTI13** (at the dose of 300 mg/kg and 2000 mg/kg BW) along with vehicle control on the brain of female Albino mice and on other highly perfused organs viz. heart, kidney, and liver tissue stained with hematoxylin and eosin (H & E) dye at the end of 14 days. The microphotographs of tissue were taken at 10X resolution.

2.9. Computational studies

2.9.1. Molecular docking

2.9.1.1. Molecular docking studies against MAO-A

Compounds **ZBTI01-ZBTI14** were docked with MAO-A using MOE software. 3D superimposition images of ligands **ZBTI01-ZBTI14** with the residues of MAO-A active site indicate proper accommodation of molecules within the gorge of active site. The naphthyl moiety of most of the compounds was oriented towards the opening of the active site while the terminal aryl ring was extended towards the bottom of the active site near the isoalloxazine ring of FAD whereas benzothiazole moiety was present in the middle of the cavity (**Figure 2.21A**). All the docked ligands occupied the same region of the active site as co-crystallized ligand harmine.

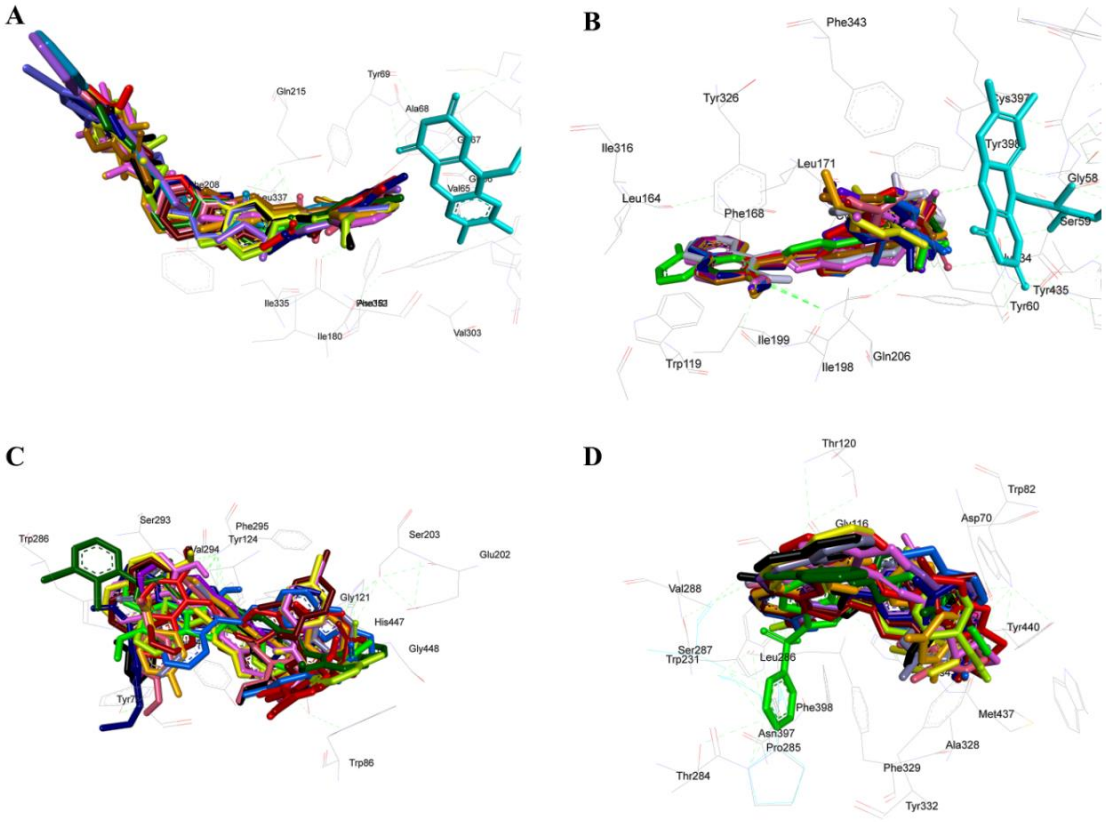

Figure 2.21. 3D superimposition image of compounds **ZBT01-ZBTI14** in the active site gorge of target proteins; A) MAO-A (PDB ID: 2Z5X) active site; B) MAO-B (PDB ID: 2V5Z) active site; C) AChE (PDB ID: 4EY7) active site and; D) BChE (PDB ID: 7AWG) active site.

Table 2.6. Molecular docking results of compounds **ZBTI01-ZBTI14** against MAOs (MAO-A/B) and ChEs (AChE/BChE)

Compd. code	MAO-A (2Z5X)		MAO-B (2V5Z)		AChE (4EY7)		BChE (7AWG)	
	ΔG (kcal/mol)	Ki (μM)	ΔG (kcal/mol)	Ki (μM)	ΔG (kcal/mol)	Ki (nM)	ΔG (kcal/mol)	Ki (μM)
ZBTI01	-12.19	0.001	-10.67	0.015	-11.32	5.030	-7.40	3.780
ZBTI02	-8.33	0.784	-9.26	0.162	-11.45	4.020	-6.15	31.180
ZBTI03	-8.45	0.640	-9.31	0.151	-12.54	0.645	-5.34	122.770
ZBTI04	-9.14	0.201	-9.15	0.195	-12.45	0.745	-7.98	1.430
ZBTI05	-8.64	0.463	-9.82	0.063	-11.85	2.070	-5.71	65.440
ZBTI06	-7.76	2.050	-8.56	0.534	-12.12	1.300	-7.93	1.540
ZBTI07	-7.67	2.400	-7.73	2.150	-11.25	5.640	-6.19	29.190
ZBTI08	-7.72	2.200	-9.33	0.144	-11.12	7.100	-5.65	72.240
ZBTI09	-8.69	0.425	-9.10	0.215	-12.10	1.350	-10.22	0.032
ZBTI10	-10.01	0.046	-6.63	13.87	-12.30	0.961	-12.23	0.001
ZBTI11	-8.53	0.562	-9.43	0.122	-12.69	0.503	-11.49	0.004
ZBTI12	-8.60	0.500	-7.69	2.32	-12.47	0.719	-11.99	0.002
ZBTI13	-11.96	0.002	-9.29	0.154	-13.31	0.176	-11.46	0.004
ZBTI14	-8.75	0.385	-9.77	0.068	-12.23	1.090	-11.15	0.007
Std.[a]	-7.34	4.160	-8.95	0.280	-10.50	0.020	-10.11	0.040

[a] Molecular Docking score of co-crystallized ligand (MAO-A, PDB ID: 2Z5X, Harmine; MAO-B, PDB ID: 2V5Z, Safinamide; AChE, PDB ID: 4EY7, Donepezil; BChE, PDB ID: 7AWG, S6Q).

2.9.1.2. Binding analysis of compound ZBTI13 with MAO-A

The visual analysis of docked 3D images of compound **ZBTI13** and MAO-A complex indicates that compound **ZBTI13** is well accommodated within the active site and binds to the cavity of reference inhibitor harmine. The naphthyl moiety of the ligand is oriented toward the entrance of the active site while the terminal variable phenyl ring was pointed toward the isoalloxazine ring of FAD (**Figure 2.22A**). The 2D interaction image of compound **ZBTI13** shows different types of molecular interactions which indicate the formation of hydrophobic (pi-alkyl, pi-pi stacked, and pi-sulfur) interactions along with hydrogen bonding. Furthermore, some residues displayed van der Waals interactions with different regions of the ligand. The oxygen atom of the carbonyl group of acetamide interacts with Gln215 through hydrogen bonding interaction whereas the *p*-methyl group at the terminal phenyl ring interacts with Tyr69 through pi-alkyl interaction. The terminal phenyl ring of the ligand interacts with Tyr407 through pi-donor hydrogen bonding. The

benzene ring of benzothiazole moiety interacts with Cys323 and Phe208 through pi-alkyl and pi-pi stacking interactions, respectively. The thiazole ring of benzothiazole moiety interacts with Phe208 and Cys323 through pi-pi stacking and pi-sulfur interactions, respectively. In addition to the above interactions, residues Ile180, Asn181, Ile335, Leu337, Phe352 and Tyr444 interact through van der Waals interaction (**Figure 2.22B**).

2.9.1.3. Molecular docking studies against MAO-B

Molecular docking of compounds **ZBTI01-ZBTI14** was carried out with MAO-B using AutoDock Tools 4.2 software. The ligand superimposition image of compounds **ZBTI01-ZBTI14** within the active site of MAO-B indicates a proper accommodation of docked molecules within the active site gorge of the enzyme. The naphthyl moiety of most of the ligands was oriented towards the opening of the active site while the terminal aryl ring was extended towards the bottom of the active site near the isoalloxazine ring of FAD whereas the benzothiazole moiety was present in the middle of the cavity (**Figure 2.21B**). All the docked ligands occupied the same region of the active site as co-crystallized ligand safinamide.

2.9.1.4. Binding analysis of compound ZBTI13 with MAO-B

Visual examination of the docked pose of compound **ZBTI13** and MAO-B complex revealed that the inhibitor is properly lodged within the active site gorge of the enzyme cavity similar to the reference inhibitor, safinamide. The molecule is traversed well across the entrance and substrate cavity of MAO-B. The naphthyl moiety of the ligand is pointed toward the opening of the entrance cavity while the terminal aryl moiety is oriented toward the bottom of the substrate cavity near the isoalloxazine ring of the FAD co-factor (**Figure 2.22C**). Analysis of the 2D interaction map of compound **ZBTI13** indicates different types of hydrophobic (pi-alkyl, pi-pi-stacking, pi-sigma, pi-sulfur and van der Waals) interactions and hydrogen bonding interactions. The hydroxyl group of the naphthyl ring interacts

through hydrogen bonding with Gln206 and Tyr326 while the naphthyl ring interacts with Leu171, and Ile199 through pi-alkyl and pi-sigma interactions. The benzene ring of benzothiazole moiety interacts with Leu171, Cys172 and Ile198 through pi-alkyl interaction while thiazole ting of benzothiazole moiety interacts with Cys172, Ile198 and Tyr435 through pi-alkyl and pi-donor hydrogen bonding interactions, respectively. Tyr435 also interacts with the nitrogen atom of the thiazole ring sulfur atom and methylene of acetamide linker through hydrogen bonding, pi-sulfur and pi-sigma interactions, respectively. The terminal aryl ring of the ligand interacts with Tyr398 through pi-pi stacking interaction while the *p*-methyl group interacts with Tyr60, Phe343 and Tyr326 through pi-alkyl interaction. In addition to the above interactions, residues Trp119, Leu164, Phe168 and Ile316 interact through van der Waals interaction (**Figure 2.22D**).

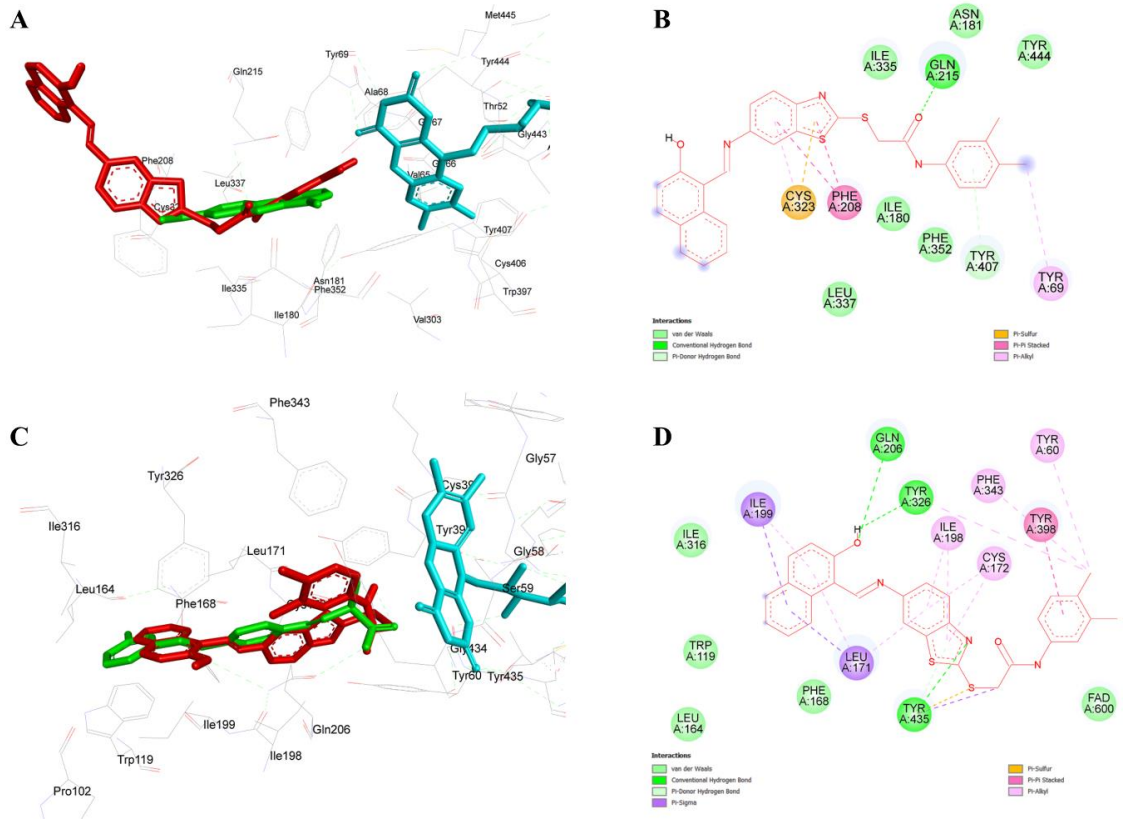

Figure 2.22. 3D binding mode and 2D interaction map of compound **ZBTI13** within the active site of MAO-A and MAO-B; A) 3D orientation of compound **ZBTI13** (red) within the active site of MAO-A along with harmine (green); B) 2D interaction of compound

ZBTI13 with active site residues of MAO-A; C) 3D orientation of compound **ZBTI13** (red) within the active of MAO-B along with safinamide (green); D) 2D interaction of compound **ZBTI13** with active site residues of MAO-B.

2.9.1.5. Molecular docking studies against AChE

A docked 3D superimposition image of compounds **ZBTI01-ZBTI14** in the active site gorge of AChE shows a good extent of accommodation within the active site. All the molecules extended throughout the active site; the terminal aryl moiety of most of the ligands is oriented towards the bottom while the naphthyl moiety of most of the ligands is pointed towards the opening of the active site and lies near the peripheral anionic site (PAS). The benzothiazole moiety of the ligands lodged in the middle of the active site along with donepezil. All the molecules occupied the same cavity same donepezil (**Figure 2.21C**).

2.9.1.6. Binding analysis of compound ZBTI13 with AChE

Visual evaluation of the docked 3D image of compound **ZBTI13** and AChE complex revealed that it is well settled within the active site and occupies the same active site region of reference inhibitor donepezil. The compound **ZBTI13** is found to traverse throughout the active site and the naphthyl moiety of the ligand is oriented towards the PAS site while the terminal aryl ring is projected towards the bottom of the site (**Figure 2.23A**). Analysis of the 2D interaction image of compound **ZBTI13** shows different types of hydrophobic interactions (pi-pi stacked, pi-pi T shaped and pi-sulfur) and hydrogen bonding interaction. The hydroxy group at naphthyl moiety interacts with Phe295 through hydrogen bonding interaction. Trp286 interacts with both rings of naphthyl moiety through pi-pi stacking interactions. The sulfur atom of the thiazole ring of benzothiazole moiety interacts with Phe338 and His447 through pi-sulfur interaction while the sulfur atom in the acetamide linker interacts with Ser203 and His447 through hydrogen bonding and pi-sulfur interactions, respectively. The benzene ring of benzothiazole moiety interacts with Tyr124 and Tyr341 through pi-donor hydrogen bonding and pi-pi T-shaped interactions,

respectively. Furthermore, the terminal phenyl ring of the ligand interacts with Tyr124 and Trp86 through pi-pi stacking interaction. Residues Tyr72, Gly121, Ser293, Val294 and Gly448 interact through van der Waals interactions (**Figure 2.23B**).

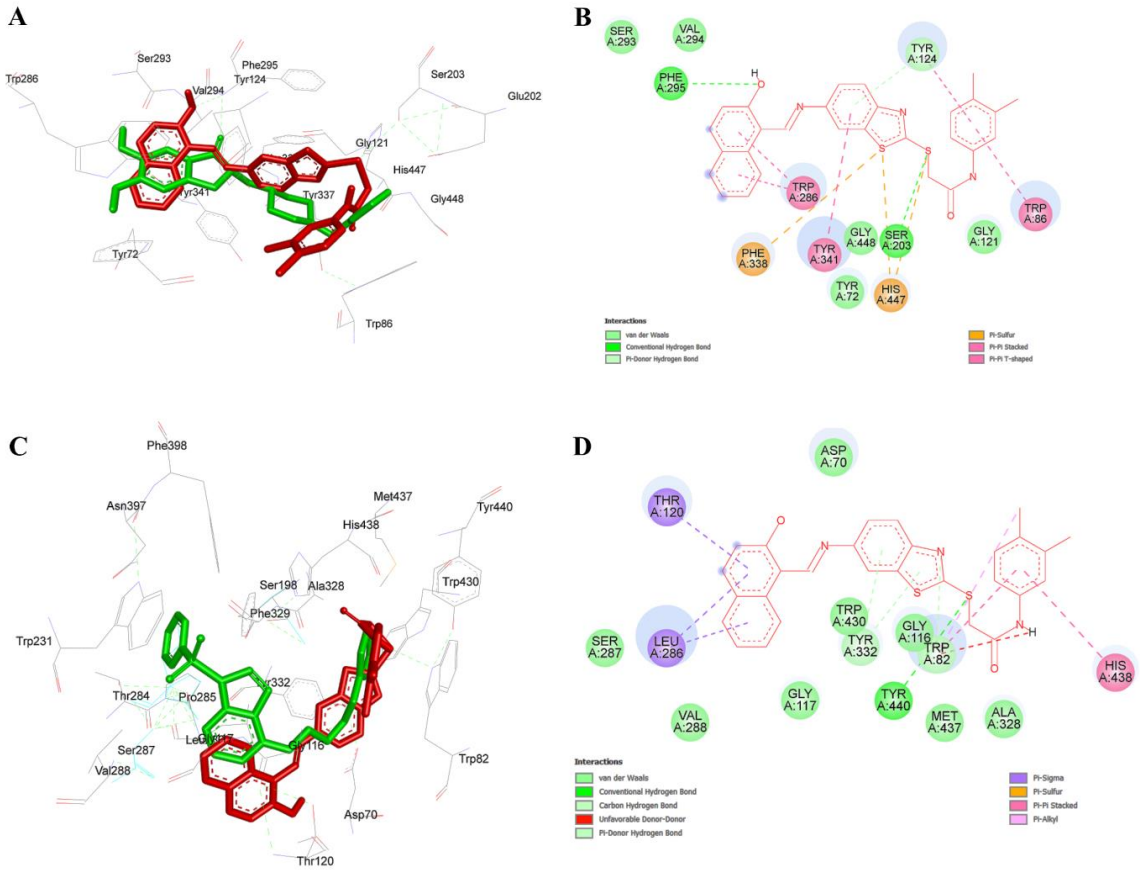

Figure 2.23. 3D orientation and 2D interaction of compound **ZBTI13** within the active site of AChE and BChE; A) 3D orientation of compound **ZBTI13** (red) within the active site of AChE along with donepezil (green); B) 2D interaction of compound **ZBTI13** with active site residues of AChE; C) 3D orientation of compound **ZBTI13** (red) within the active of BChE along with S6Q (green); D) 2D interaction of compound **ZBTI13** with active residues of BChE

2.9.1.7. Molecular docking studies against BChE

All the synthesized compounds were docked against BChE to understand the types of molecular interactions and binding patterns within the active site. The superimposition image of all docked compounds revealed the orientation of ligands within the active site gorge. The naphthyl moiety of most of the ligands was oriented toward the opening of the

active site while the terminal aryl ring was pointed toward the bottom of the active site. The benzothiazole moiety of most of the molecules was found to lie in the middle of the cavity (**Figure 2.21D**).

2.9.1.8. Binding analysis of compound ZBTI13 with BChE

Visualization of the docked 3D image of compound **ZBTI13** and BChE complex revealed that compound **ZBTI13** was well accommodated within the active site and occupied the same cavity as the reference inhibitor. The naphthyl moiety of the ligand is pointed towards the bottom of the active site while terminal aryl moiety is oriented towards the opening of the gorge (**Figure 2.23C**). The 2D interaction image of compound **ZBTI13** shows different types of molecular interaction that stabilize the ligand. Both rings of naphthyl moiety interact with Thr120 and Leu286 through pi-sigma interaction. The sulfur atom of the acetamide linker interacts with Tyr440 through hydrogen bonding interaction while the terminal phenyl ring interacts with Trp82 and His438 through pi-pi stacking interaction. The benzothiazole moiety of ligand interacts with Tyr332 and Trp82 through pi-donor hydrogen bonding interaction. Additionally, residues Asp70, Gly116, Gly117, Ser287, Val288, Ala328 and Trp430 interact through van der Waals interactions (**Figure 2.23D**).

2.9.2. Molecular dynamic simulation

Protein-ligand complexes were evaluated for their stability by different parameters including root mean square deviation (RMSD), ligand-protein contacts, protein-ligand contact histogram, and protein-ligand contact timeline along with root mean square fluctuation (RMSF) of the protein and ligand complex. Further, the secondary structure elements (SSE) of the protein like α-helices and β-strands, the torsional profile of the ligand and properties like the radius of gyration (rGyr), intramolecular hydrogen bonding (intraHB), polar surface area (PSA), solvent accessible surface area (SASA) were analyzed for any significant conformational change in the protein structure during the simulation.

2.9.2.1. MD simulation of compound ZBTI13 -MAO-B complex

Visual analysis of MD simulation results shows that compound **ZBTI13** was well accommodated within the active site of MAO-B and stabilized by the formation of different types of molecular interactions including hydrogen bonding and hydrophobic interaction along with water bridges. Compound **ZBTI13** formed hydrogen bond with Ser59, Tyr60, Ile199, Ser200, Thr201 and Tyr326. Residues Ile14, Leu88, Phe99, Phe103, Trp119, Leu164, Leu167, Phe168, Leu171, Ile198, Ile199, Ile316, Tyr326, Phe343, Tyr398, Tyr435 and Met436 interact through hydrophobic interaction while residues Ser59, Leu171, Cys172, Ile199, Ser200, Thr201, Gln206, Lys296, Tyr326, Tyr398, Gly434 and Tyr435 interact by forming water bridge (**Figure 2.24B & 2.24D**). A good degree of contact was observed between the ligand and target protein throughout the simulation period with Ser59, Tyr60, Leu171, Ile199, Thr201, Ile316, Tyr326, Phe343, Gly434 and Met436 (**Figure 2.24A**). RMSD graph of compound **ZBTI13** indicates that it was in the acceptable range (1-3 Å) and the ligand was well stabilized during the simulation period. From the RMSD graph, it is also clear that the protein and ligand both were stable and no conformational change occurred during the simulation process (**Figure 2.24C**).

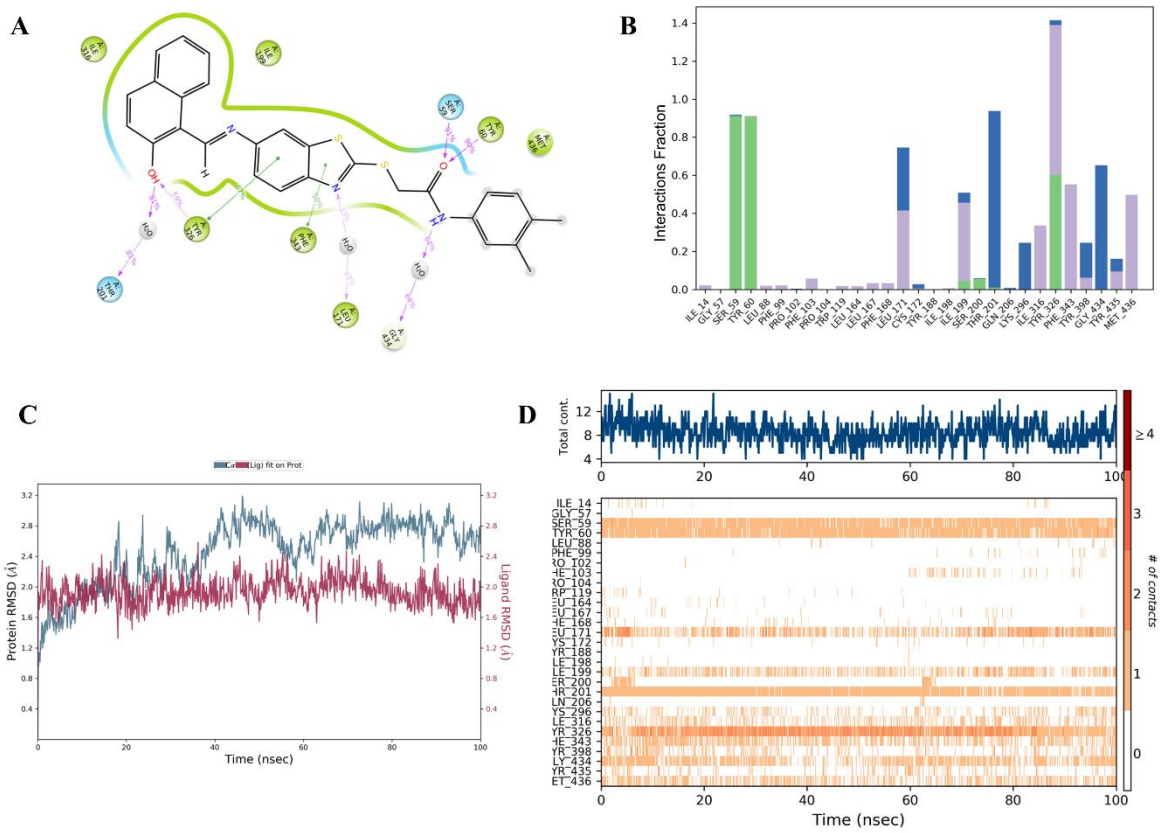

Figure 2.24. Protein-ligand contacts generated during MD simulation of compound **ZBTI13** with MAO-B (PDB ID: 2V5Z); A) 2D interaction diagram indicated percent interaction with surrounding residues; B) Different types of protein-ligand contacts are represented by stacked bar chart; C) RMSD graph of protein (blue) and ligand (maroon); D) Protein-ligand contacts timeline diagram.

2.9.2.2. MD simulation of compound ZBTI13-AChE complex

Visualization of MD simulation results of compound **ZBTI13** and AChE complex shows that the molecule was stabilized by hydrogen bonding and hydrophobic interactions with surrounding active site residues in addition to water bridges. Compound **ZBTI13** was stabilized by hydrogen bonding with Leu76, Tyr124, Leu289, Gln291, Glu292, Tyr341 and Gly342. Residues Tyr72, Leu76, Trp86, Tyr124, Trp286, His287, Val294, Phe295, Phe297, Tyr337, Phe338, Tyr341, Pro344 and Val365 interacts through hydrophobic interaction. Residues Tyr72, Asp74, Leu76, Tyr124, Trp286, His287, Leu289, Pro290, Gln291, Glu292, Ser293, Phe295, Arg296, Tyr341 and Arh364 interact with ligands by forming water

bridges (**Figure 2.25B**). Phe297 and Tyr341 interact with ligands through pi-pi stacking for 38 % and 77 % of the total simulation period while residues Trp286 and Val365 interact through hydrophobic interaction (**Figure 2.25A**). The RMSD graph of protein and ligand indicates that compound **ZBTI13** was highly stable from 20 to 80 ns out of the 100 ns simulation period. The RMSD graph does not show any conformational change during the simulation process (**Figure 2.25C**). The protein-ligand contact timeline diagram shows crucial amino acid residues (Trp286 and Tyr341) (**Figure 2.25D**).

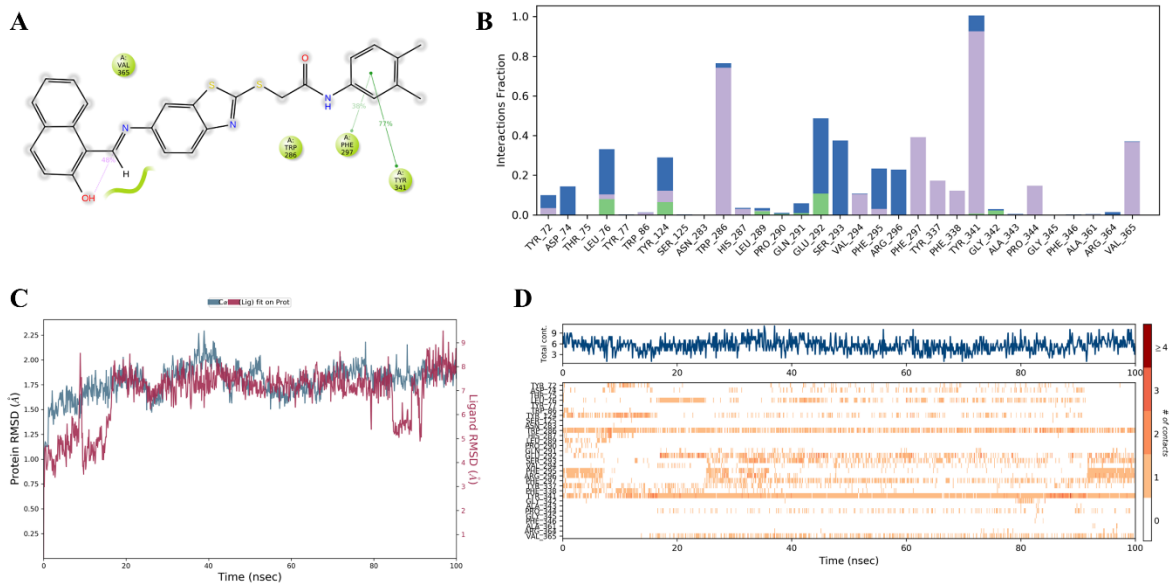

Figure 2.25. Protein-ligand contacts generated during MD simulation of compound **ZBTI13** with AChE (PDB ID: 4EY7); A) 2D interaction diagram indicated percent interaction with surrounding residues; B) Different types of protein-ligand contacts are represented by stacked bar chart; C) RMSD graph of protein (blue) and ligand (maroon); D) Protein-ligand contacts timeline diagram.

2.9.3. Comparative analysis of docking and MDS studies

The results of molecular docking studies and molecular dynamic simulation studies were compared to understand the reliability and robustness of crucial molecular interactions that are important for the stability of the protein-ligand complex. The hydrogen bonding formed by Tyr60, Ile199 and Tyr326 in molecular docking of compound **ZBTI13** with MAO-B

was also retained in MD simulation and two additional hydrogen bonds were formed by Ser59 and Ser200. The hydrophobic interaction formed by residues Leu171, Ile199 and Ile316 in molecular docking of compound **ZBTI13** with MAO-B remained unchanged during MD simulation while van der Waals interactions formed by residues Leu167, Phe168, Cys172, Ile198, Tyr326 and Tyr435 in molecular docking were observed as hydrophobic interaction during MD simulation. The hydrogen bonding formed by residues Tyr133 and Phe295 in molecular docking of compound **ZBTI13** with AChE were observed as hydrophobic interactions during MD simulation while hydrophobic interactions formed by Trp86, Trp286, Tyr337, Phe338 and Tyr341 residues during molecular docking remained unchanged in MD simulation study. From the above comparison, it can be concluded that compound **ZBTI13** was well accommodated in both molecular docking and MD simulation studies and also formed an interaction that stabilized it more efficiently than found in the docking study.

2.9.4. Ligand binding efficiency

Ligand efficiency is the ratio of free energy of binding over the number of heavy atoms in a ligand. The number of heavy atoms in the ligand and their size have an impact on the potency of the molecule and are regarded as an important metric in drug discovery. After a certain extent, an increase in the number of heavy atoms compromises the potency of the ligand due to an increase in the total polar surface area. A very low or very high number of heavy atom counts is not suitable for a ligand to be an efficient binder. The ligand binding efficiency of compounds **ZBTI01-ZBTI14** was calculated through the MedChem calculator web server (http://www.vulpinescience.co.uk/uploads/MedChem%20Calculators_Ver3.2/MedChem%20Calculators.htm). The ligand binding efficiency of most of the molecules lies near 0.3 and reference inhibitors also fall in the same region which shows that the number of heavy

atoms present in the compounds **ZBTI01-ZBTI14** are in the acceptable range (**Figure 2.26**) [29].

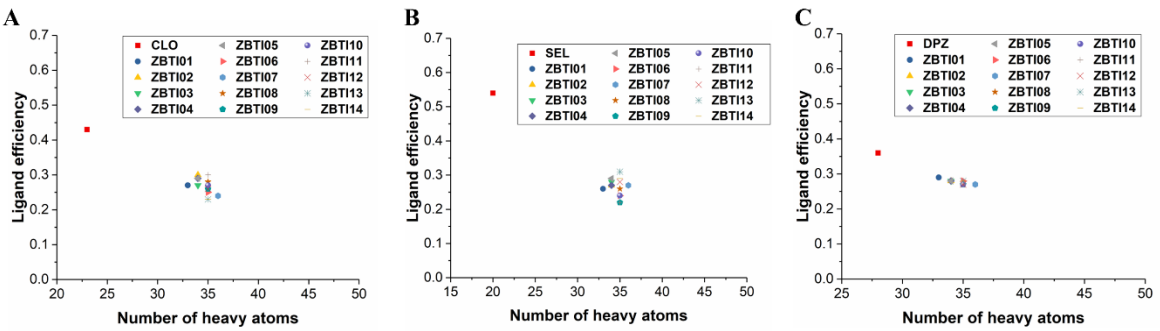

Figure 2.26. Ligand binding efficiency of compounds **ZBTI01-ZBTI14** and reference standard inhibitors of MAO-A (clorgyline), MAO-B (selegiline) and AChE (donepezil).

2.9.5. Predicted ADMETox parameters

ADMET properties of all the synthesized compounds were predicted to understand the pharmacokinetic profile of the compounds. The prediction gives us an insight into how these molecules will behave when injected into the living system. Predicted human intestinal absorption of all the compounds was found between 95 % and 97 % and falls in the good absorption range while skin permeability of most of the compounds falls between -2.20 and -3.17 which indicates that compounds are not suitable for transdermal administration. Each compound showed moderate absorption for Caco2 cells whereas poor absorption for MDCK cells. All the compounds showed strong plasma protein binding and low blood-brain barrier permeability. All the compounds were predicted as inhibitors of both enzymes CYP2C9 and CYP3A4 while non-inhibitors of CYP2C19 (**Table 2.7**).

Table 2.7. Predicted ADME parameters of compounds **ZBTI01-ZBTI14**

Compd. code	HIA (%)	Caco2	MDCK (nm/s)	SP (logKp, cm/h)	BBB	PPB (%)	CYP2C9	CYP2C19	CYP3A4
ZBTI01	96.66	31.96	0.491	-2.56	0.027	97.66	inhibitor	non	inhibitor
ZBTI02	96.66	34.51	0.420	-2.66	0.036	94.70	inhibitor	non	inhibitor
ZBTI03	97.16	34.75	0.596	-2.51	0.045	94.32	inhibitor	non	inhibitor
ZBTI04	97.45	29.43	0.020	-2.52	0.047	91.24	inhibitor	non	inhibitor
ZBTI05	95.31	21.38	0.235	-3.17	0.040	94.72	inhibitor	non	inhibitor
ZBTI06	96.76	33.16	0.939	-2.34	0.036	97.56	inhibitor	non	inhibitor

ZBTI07	96.44	34.95	0.421	-2.53	0.042	97.02	inhibitor	non	inhibitor
ZBTI08	96.50	38.37	0.880	-2.38	0.042	95.43	inhibitor	non	inhibitor
ZBTI09	96.67	36.45	1.635	-2.72	0.049	91.88	inhibitor	non	inhibitor
ZBTI10	96.67	36.44	7.740	-2.69	0.050	91.46	inhibitor	non	inhibitor
ZBTI11	97.57	36.42	0.088	-2.42	0.080	92.86	inhibitor	non	inhibitor
ZBTI12	97.57	36.83	0.542	-2.43	0.087	93.21	inhibitor	non	inhibitor
ZBTI13	96.87	35.06	0.165	-2.22	0.057	97.28	inhibitor	non	inhibitor
ZBTI14	96.87	34.46	0.659	-2.20	0.055	96.50	inhibitor	non	Inhibitor
CLO	100.00	52.49	2.184	-1.30	6.737	81.07	Non	Non	Non
SEL	100.00	31.94	164.082	-0.79	4.435	53.20	Non	Inhibitor	Non
PCPA	100.00	21.11	127.21	-2.16	0.640	1.76	Inhibitor	Inhibitor	Inhibitor
DPZ	97.95	55.51	0.138	-3.04	0.187	84.61	Non	Non	Non

HIA = Human intestinal absorption (%), Rule: 0-20 (poor), 20-70 (moderate) and 70-100 (well); **Caco2** = *In vitro* permeability of Caco2 cell (nm/s), Rule: <4 (low), 4-70 (moderate), >70 (high); **MDCK** = Maden Darby canine kidney cell permeability (nm/s), Rule: <25 (low), 25-500 (moderate), >500 (high); **SP**: *In vitro* skin permeability (cm/h); **BBB** = Blood brain barrier permeability (C_{brain}/C_{blood}), Rule: <0.1 (low), 0.1-2.0 (moderate), >2.0 (High); **PPB** = *In vitro* plasma protein binding (%), Rule: <90 (moderate bound), >90 (Strong bound); Non = non inhibitor.

Additionally, compounds **ZBTI01-ZBTI14** were predicted for their mutagenicity using the Ames test, mouse and rat carcinogenicity and hERG inhibition. All the compounds were predicted as mutagens except compound **ZBTI10** against the Ames test whereas the mouse carcinogenicity was predicted as negative except compound **ZBTI02** and **ZBTI08** [36]. Rat carcinogenicity was predicted negative for all compounds except **ZBTI04**. All the compounds have a high risk for hERG inhibition except compound **ZBTI01** predicted as ambiguous which indicates that our compounds may exert cardiotoxicity (**Table 2.8**) [33].

Table 2.8. Predicted toxicity parameters of compounds **ZBTI01-ZBTI14**

Compound Code	Ames test	Carcinogenicity (Mouse)	Carcinogenicity (Rat)	hERG inhibition
ZBTI01	Mutagen	Negative	Negative	Ambiguous
ZBTI02	Mutagen	Positive	Negative	High risk
ZBTI03	Mutagen	Negative	Negative	High risk
ZBTI04	Mutagen	Negative	Positive	High risk
ZBTI05	Mutagen	Negative	Negative	High risk
ZBTI06	Mutagen	Negative	Negative	High risk
ZBTI07	Mutagen	Negative	Negative	High risk
ZBTI08	Mutagen	Positive	Negative	High risk
ZBTI09	Mutagen	Negative	Negative	High risk
ZBTI10	Non-mutagen	Negative	Negative	High risk
ZBTI11	Mutagen	Negative	Negative	High risk
ZBTI12	Mutagen	Negative	Negative	High risk
ZBTI13	Mutagen	Negative	Negative	High risk
ZBTI14	Mutagen	Negative	Negative	High risk

CLO	Mutagen	positive	Negative	Medium risk
SEL	Mutagen	Negative	Negative	Medium risk
PCPA	Mutagen	positive	Negative	Medium risk
DPZ	Mutagen	Negative	Negative	Medium risk

Ames test-Ames test for mutagenicity in *Salmonella typhimurium*, **Carcinogenicity (Mouse)**-2 years carcinogenicity bioassay in mouse, **Carcinogenicity (Rat)**-2 years carcinogenicity bioassay in rat, **hERG Inhibition**-*In vitro* Human Ether-a-go-go Related Gene Channel Inhibition.

2.10. Summary

In summary, the pharmacophore-based virtual screening study was performed on the ZINC15 database (a free database of commercially available compounds for virtual screening containing over 230 million purchasable compounds) against a pharmacophore query built around the hypothetical space in safinamide (a potent and reversible MAO-B inhibitor) using MOE software. The ZINC15 database was screened against the built pharmacophore model query using the Pharmit web server by applying an appropriate molecular filter and identifying 225 molecules. The obtained results from 225 molecules were subsequently filtered for drug-likeness and PAINS-Remover to yield 177 virtual hits. These virtual hits were further screened by molecular docking and MD simulation studies which resulted in **ZINC02181408** as the most active virtual lead (S score = -10.81 kcal/mol). The synthesis of the virtual lead was accomplished by retrosynthetic methodology along with 13 other structural analogs. The synthesized compounds were characterized by FTIR, NMR, HRMS and HPLC analysis and evaluated against ratMAO-A, ratMAO-B, *ee*AChE, and *eq*BChE enzymes where compound **ZBTI11** emerged as the most potent MAO-A inhibitor (IC_{50} = 0.030 ± 0.008 μM) whereas compound **ZBTI13** emerged as the most potent dual MAO-B and AChE inhibitor (MAO-B IC_{50} = 0.015 ± 0.007 μM, AChE IC_{50} = 0.114 ± 0.003 μM; competitive reversible inhibitor of MAO-B and mixed reversible inhibitor of AChE). Computational studies revealed that the lead molecule **ZBTI13** strongly binds to the active sites of the target enzymes and is stabilized by H-bonding and hydrophobic interactions. Further, selected compounds were evaluated for

antioxidant potential among which compound **ZBTI04** showed maximum % FRS while metal chelation assay resulted in compounds **ZBTI11**, **ZBTI13** and **ZBTI14** as chelators of iron. The blood-brain-barrier permeability study of compound **ZBTI13** revealed ambiguous permeability of the compound. Additionally, cell-based studies were carried out against fibroblast (L929) and neuroblastoma (SH-SY5Y) cells to evaluate the *in vitro* toxicological profile of lead compound **ZBTI13** and was found to be non-toxic up to 10 μM concentration in fibroblast while up to 50 μM in neuroblastoma cells. Moreover, the *in vivo* neuroprotective efficacy of the compound **ZBTI13** was evaluated against the scopolamine-induced amnesia model using Albino mice. The observed *in vivo* results suggest the neuroprotective potential of the compound **ZBTI13** whereas *ex vivo* results indicate a reversal of ACh, AChE, MDA and CAT levels in the **ZBTI13**-treated group as compared to the scopolamine-treated group. The prediction of pharmacokinetic parameters and toxicity of compounds **ZBTI01-ZBTI14** suggest a high risk for hERG inhibition which indicates that our compounds may exert cardiotoxicity (**Figure 2.27**).

Overall, the attempted PBVS-based virtual screening and subsequent experimental validation screening study afforded a new benzothiazole-based compound (**ZBTI13**) that displayed nanomolar MAO-B inhibitory potency along with potential multifunctional properties.

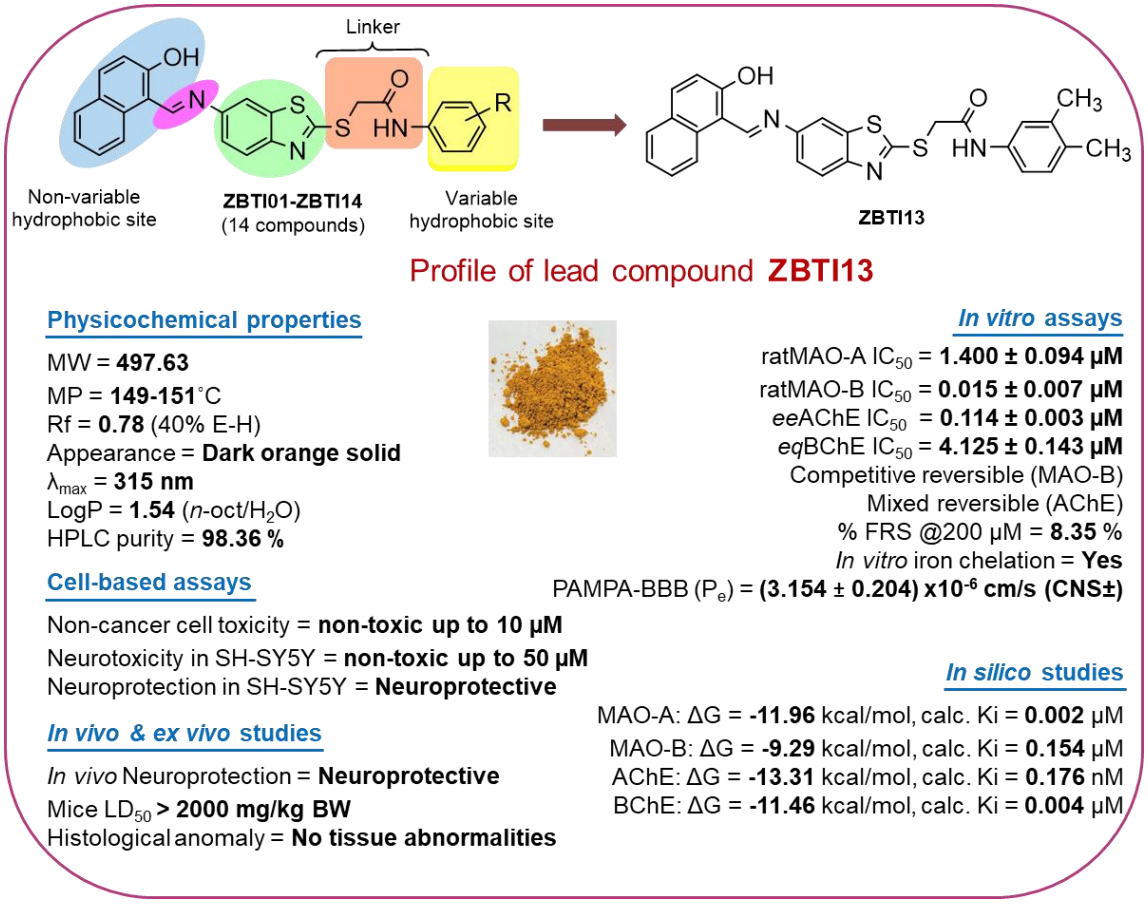

Figure 2.27. Summary of key outcomes from the **ZBTI series**